NASA CR-174768
GTD 84-4

INVESTIGATION OF A

PULSED ELECTROTHERMAL THRUSTER SYSTEM

by R. L. Burton, S. A. Goldstein, B. V. Hilko
D. A. Tidman and N. K. Winsor

GT-DEVICES, INC.

prepared for

NATIONAL AERONAUTICS AND SPACE ADMINISTRATION

NASA Lewis Research Center
Contract NAS 3-23866

1. Report No.	2. Government Accession No.	3. Recipient's Catalog No.
CR 174768		

4. Title and Subtitle	5. Report Date
Investigation of a Pulsed Electrothermal Thruster System	October 31, 1984
	6. Performing Organization Code

7. Author(s)	8. Performing Organization Report No.
R. L. Burton, S. A. Goldstein, B. K. Hilko, D. A. Tidman and N. K. Winsor	GTD Report No. 84-4
	10. Work Unit No.

9. Performing Organization Name and Address	11. Contract or Grant No.
GT-Devices, Inc. 5705A General Washington Drive Alexandria, VA 22312	NAS3-23866
	13. Type of Report and Period Covered Contract Report

12. Sponsoring Agency Name and Address	14. Sponsoring Agency Code
National Aeronautics and Space Administration Washington, DC 20546	

15. Supplementary Notes

Project Manager, Shih-Ying Wang, Space Propulsion Technology Division
NASA Lewis Research Center

16. Abstract

The performance of an ablative-wall Pulsed Electrothermal (PET) thruster is accurately characterized on a calibrated thrust stand, using polyethylene propellant. The thruster is tested for four configurations of capillary length and pulse length, ranging from a 15 cm capillary driven by a 15 μsec pulse (unsteady mode) to a 4.5 cm capillary driven by a 100 μsec pulse (quasi-steady mode). The exhaust velocity is determined with twin time-of-flight photodiode stagnation probes, and the ablated mass is measured from the loss over ten shots. Based on the measured thrust impulse and the ablated mass, the specific impulse varies from 1000 to 1750 seconds. The thrust to power varies from .05 N/kW (quasi-steady mode) to .10 N/kW (unsteady mode). The thruster efficiency varies from .56 at 1000 seconds to .42 at 1750 seconds.

A conceptual design is presented for a 40 kW PET propulsion system, capable of orbit raising of a 7000 kg Space Based Radar in 15 days with ΔV = 1000 m/sec. The point design system performance is .62 system efficiency at 1000 seconds specific impulse. The system's reliability is enhanced by incorporating 20, 20 kW thruster modules which are fired in pairs. The thruster design is non-ablative, and uses water propellant, from a central storage tank, injected through the cathode. System dry mass is extrapolated from existing space-qualified hardware, and is estimated to be 10 kg/kW.

17. Key Words (Suggested by Author(s))	18. Distribution Statement
Electric Propulsion Electrothermal Thruster Thruster Performance Electric Propulsion Systems	Unclassified-Unlimited

19. Security Classif. (of this report)	20. Security Classif. (of this page)	21. No. of Pages	22. Price*
Unclassified	Unclassified	64	

* For sale by the National Technical Information Service, Springfield, Virginia 22161

TABLE OF CONTENTS

SUMMARY

Pulsed Electrothermal (PET) propulsion is a technique for avoiding the material temperature limitations of steady electrothermal propulsion, by operating at megawatt power levels for microsecond time scales, with the time between pulses measured in milliseconds. By varying the energy per pulse and the pulse rate, operating parameters can always be found which prevent the electrodes from reaching the melting point. A second benefit of pulsed operation comes from the 1000 atmosphere pressure levels achieved during the pulse. The supersonic nozzle flow is then in an equilibrium rather than a frozen state, so that the ionization energy of the propellant is recovered in the nozzle. In addition, the high Reynolds number in the nozzle allows the nozzle flow to be treated as inviscid.

This report is divided into two parts. Part one is an experimental study of an ablative wall PET thruster, using polyethylene propellant. In order to achieve high confidence in the performance measurements, a calibrator is used in conjunction with the thrust stand, and twin time-of-flight probes are used to measure exhaust velocity. Energy delivered is measured from the time-integrated product of terminal current and voltage, and mass loss is determined with a highly accurate balance. The performance parameters are determinded by averaging the results for a ten shot series under constant conditions.

The thruster is tested with four configurations of capillary length and pulse length. A 15 cm long capillary and 15 μsec pulse are used to produce the unsteady mode condition, for which

the acoustic time in the capillary is greater than the pulse length tp ($ctp/2\ell < 1$). Quasi-steady conditions are created with 4.5 cm and 5.5 cm capillaries, used with 48 μsec and 100 μsec pulses, for which $ctp/2\ell >> 1$.

As expected, the thruster runs at a relatively low average temperature in the unsteady mode, resulting in a 1000 sec specific impulse. The thrust to power ratio is .10 N/kW, and the thruster efficiency is .56. A large fraction of the exhaust mass in this mode exists as "afterglow" in the tail of the pulse.

Longer pulses(quasi-steady mode) are tested to reduce the relative effect of the afterglow. The 48 μsec and 100 μsec pulses result in a 1500 to 1750 second specific impulse. The thrust to power ratio falls to .05 N/kW, and the efficiency averages .40. The exhaust velocity is measured as 27 km/sec, indicating that the afterglow effect is still important for the quasi-steady mode.

Part II of the report addresses the propellant feed problem, and proposes a PET propulsion design for an orbit-raising mission. A conceptual design of a 40 kW PET system is presented for a Space-Based Radar satellite. The selected mission is orbit raising of the 7000 kg SBR satellite in 15 days with a characteristic velocity of ΔV = 1000 m/sec. The point design system performance is .62 efficiency at 1000 seconds. The system's reliability is enhanced by incorporating 20 thruster modules of 20 kW each, fired in pairs. The thruster design is non-ablative, and uses water propellant from a central storage tank, injected through the cathode. System dry mass is

extrapolated from existing space-qualified hardware, and is estimated to be 10 kg/kW.

I. INTRODUCTION

In a previous report[1] we presented performance data for an ablative wall, pulsed electrothermal (PET) thruster. In that device, a 2 kJ electric discharge was used to create a polyethylene or Teflon plasma at a pressure of about 700 atm and a temperature of 2.5 eV. From current, voltage, impulse bit, exhaust velocity and mass loss measurements, we concluded that the PET thruster gives repeatable results, operates with equilibrium flow in the nozzle, and substantially recovers the plasma ionization energy. Based on calculations of losses from evaporation, dissociation, and unrecoverable thermal energy, these results demonstrated that the PET thruster has the potential of achieving efficiencies in the .70 to .80 range at 2000 seconds specific impulse.

The next steps in PET thruster development are discussed in this report. In the first report[1], it was concluded that refinements in the performance measurement techniques could be easily made that would increase accuracy and confidence in the results. We have therefore developed a precise calibration system that simulates the impulse bit with an overall accuracy of better than 1%. We have also used twin photodiode probes to improve the exhaust velocity measurement, and have improved the thrust stand design to reduce mechanical noise on the thrust signal. Improvements have also been made in the technique for measuring mass loss.

The second important step for PET thruster development, addressed in this report, is to solve the propellant feed problem. Although solid propellant feed systems for the Teflon Pulsed Plasma Thruster have been successfully developed and orbited, it was not at all clear that this could be easily done for the PET thruster's coaxial geometry. As a focus for a feed system conceptual design effort, it was decided to select a representative mission, for which the PET thruster is particularly attractive. The result of this study is a 40 kW PET propulsion system for the Lincoln Labs' Space Based Radar, using water propellant. The results of the experimental effort and the conceptual design are presented below and in Appendix A.

II. PET THRUSTER PERFORMANCE MEASUREMENTS

In a previous report[1], diagnostic techniques for PET thruster performance measurements were discussed in detail. This discussion is summarized in Appendix A of this report. We have since developed several techniques for refining the PET thruster performance measurements.

The performance of the PET thruster is defined through five primary diagnostic techniques. These are:

1. Discharge current, measured by an RC integrated Rogowski loop.
2. Discharge voltage, measured by a resistive 935:1 voltage divider.
3. Impulse bit, measured by the recoil momentum of the thrust stand.
4. Exhaust velocity, measured by time-of-flight to three types of probes at different positions in the exhaust stream.
5. Mass loss, determined by accurate weighing of the discharge liner, cathode, and nozzle.

Typical profiles for current, voltage, impulse bit, and exhaust velocity probes are shown in Figures 1-3. The analysis of PET thruster performance is based on terminal measurements. The current and voltage are multiplied to give input power (Fig. 1) and then integrated to give the delivered energy, E_D. Typically, the discharge resistance is at least ten times larger than the external resistance, so that $E_D/(1/2CV_0^2) > 0.9$. The slope of the recoil signal (Fig. 2) is determined graphically,

GTD

PET THRUSTER TERMINAL MEASUREMENTS

POLYETHYLENE PROPELLANT
5.5cm CAPILLARY
1.8kJ DELIVERED

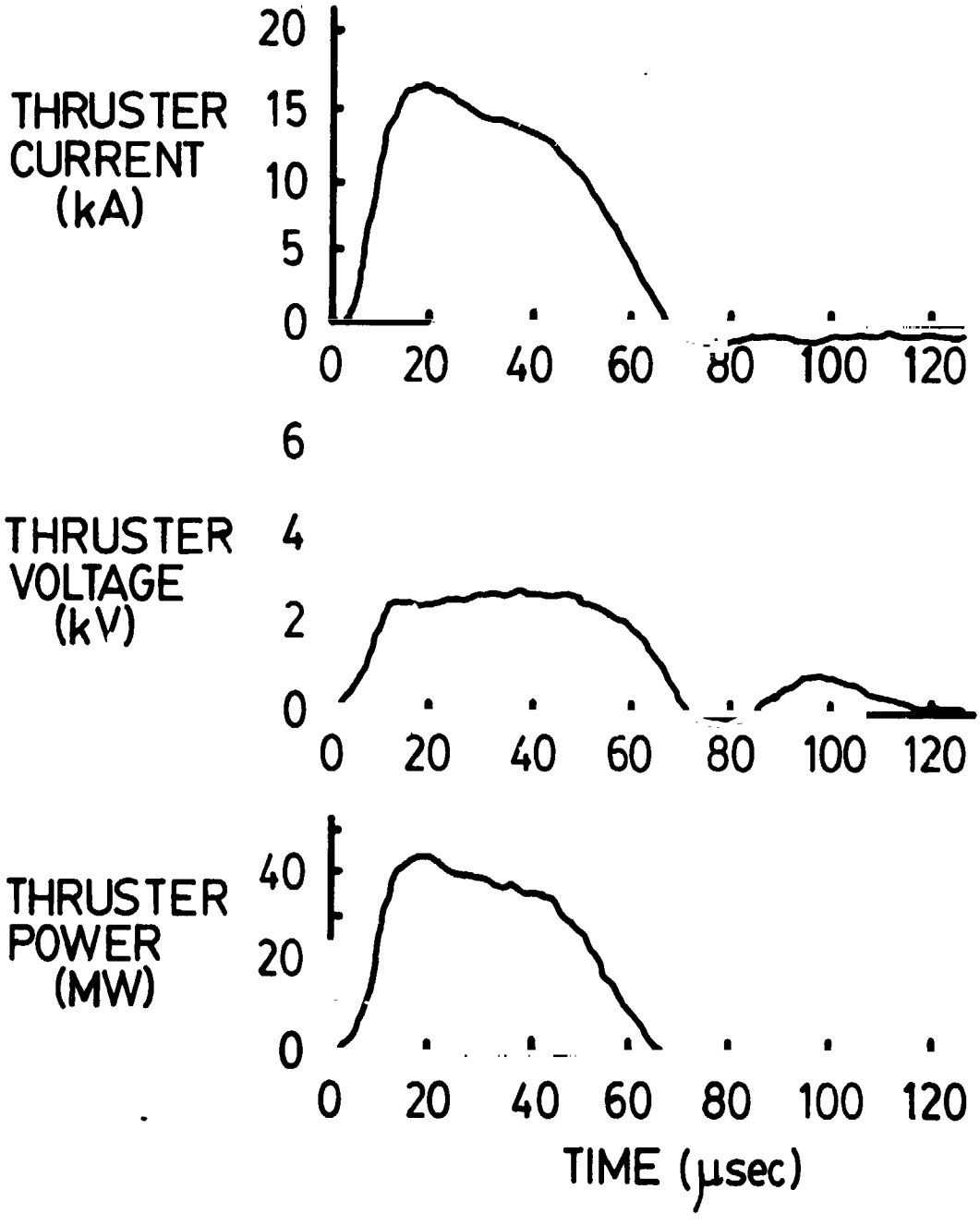

Figure 1

GTD

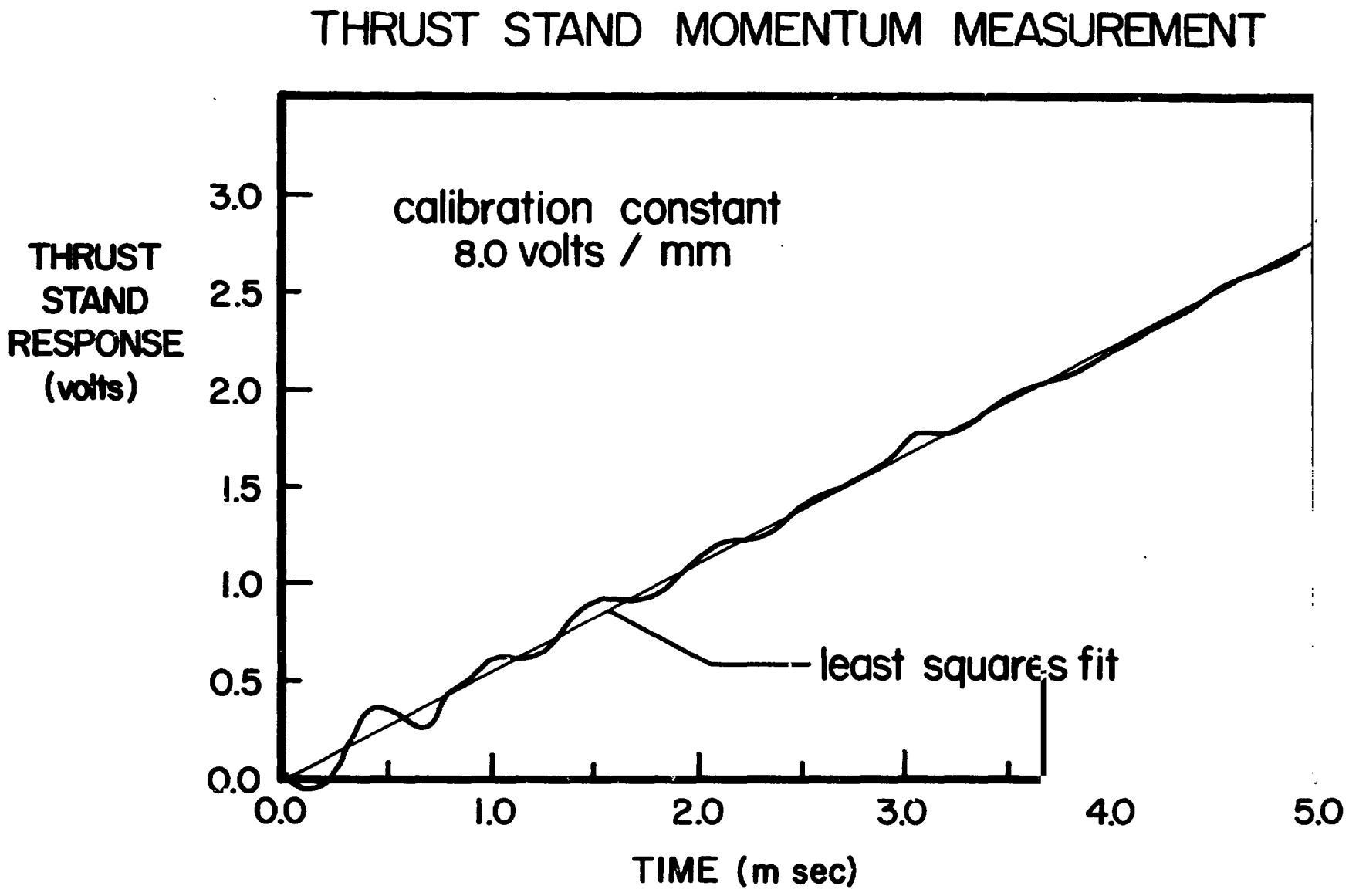
THRUST STAND MOMENTUM MEASUREMENT
calibration constant
8.0 volts / mm
THRUST
STAND
RESPONSE
(volts)
3.0
2.5
2.0
1.5
1.0
0.5
0.0
least squares fit
0.0
1.0
2.0
3.0
4.0
5.0
TIME (m sec)

Figure 2

GTD

PHOTODIODE PROBE RESPONSE vs POSITION

POLYETHYLENE
5.5cm CAPILLARY
1.8 kJ DELIVERED

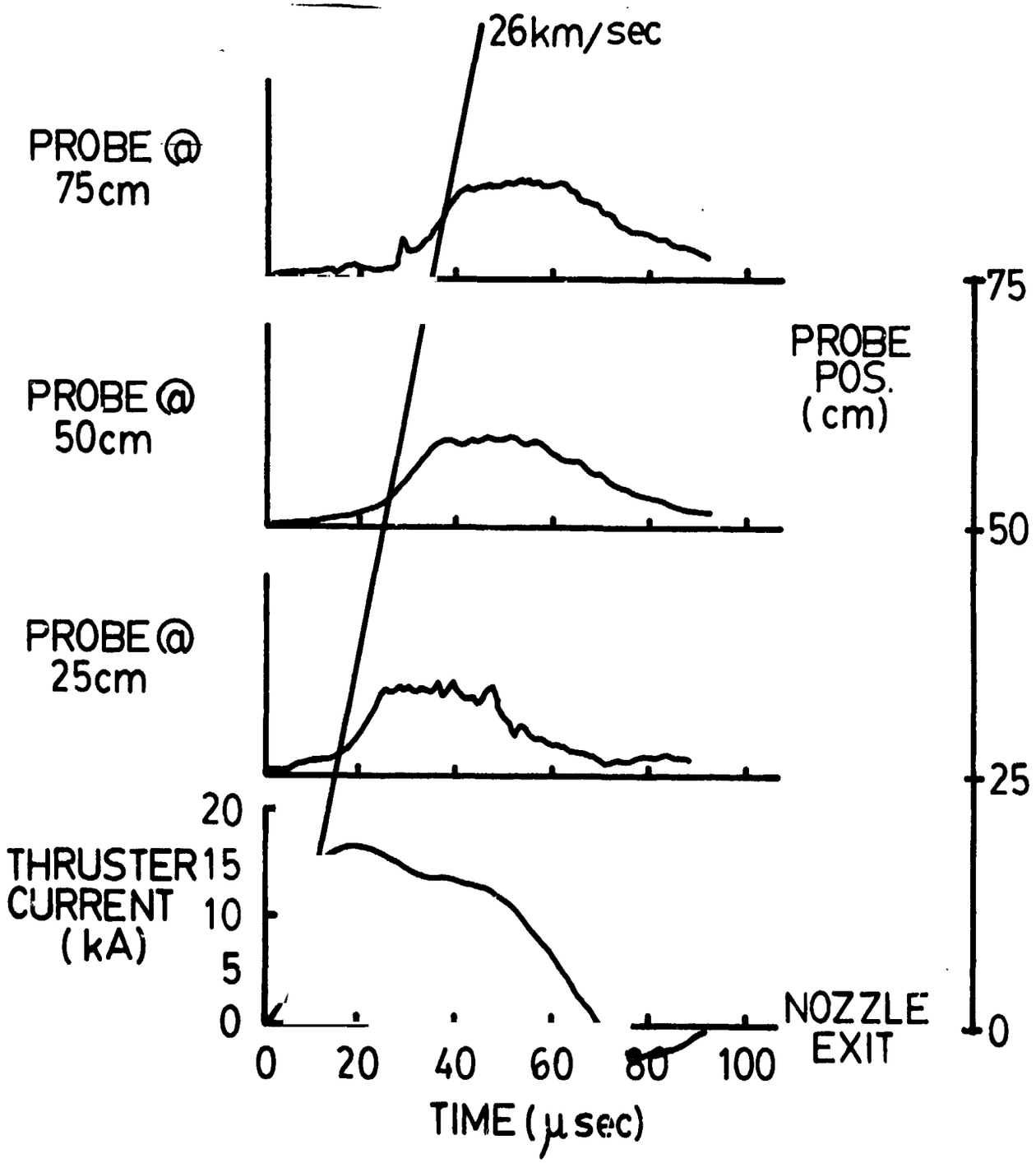

Figure 3

and is multiplied by the recoil mass to give impulse bit. These two measurements immediately give the thrust to power ratio T/P from

$$\frac{T}{P}\,[N/W] = \frac{\int T dt}{E_D}\ \frac{[N\text{-}s]}{[J]}$$

Previously reported results for polyethylene propellant have given values of T/P ranging from .05 [N/kW] to .10 [N/kW] depending on the pulse length.

The exhaust velocity and mass loss measurements are required to determine specific impulse and thruster efficiency. Their product should be equal to the measured impulse bit:

$$\int T dt = \Delta m u_e$$

As was shown previously, however, the quantity $\Delta m u_e$ exceeds the impulse bit $\int T dt$ by nearly a factor of 2. The explanation for this discrepancy is that the mass velocity measured by the time-of-flight exhaust probes is higher than the mean mass velocity for the entire pulse. In support of this, a computational model of the discharge shows that about two-thirds of the mass is ejected at high temperature during the pulse, and one third is ejected at much lower temperature and velocity in the pulse "afterglow" (Fig. 4).

Since the afterglow portion of the pulse reduces the mean exhaust velocity, it was decided to minimize the importance of the afterglow by increasing pulse length. We report here on two test series, of ten shots each, using polyethylene propellant. One series was run with a 48 μsec pulse, duplicating the 48 μsec tests reported earlier[1]. The second series was run with the same capillary geometry but with a 100 μsec pulse. The results

GTD

COMPUTED CAPILLARY MASS LOSS

polyethylene
quasi-steady, 2kJ
shot P077

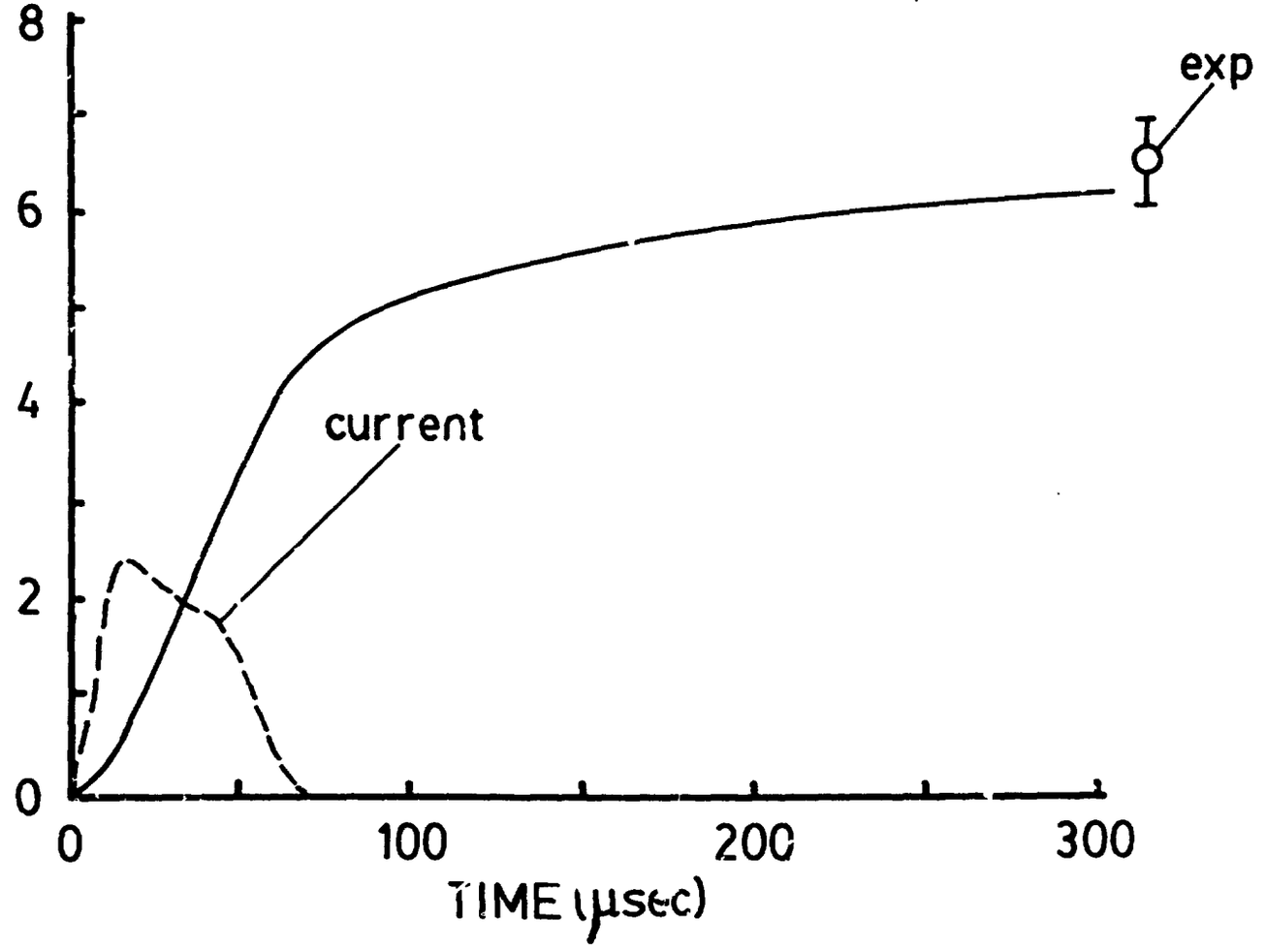

Figure 4

of these tests are summarized below, and are reported in more detail in Appendix A.

Since a major goal of the present experiments is to improve measurement accuracy, new approaches were taken to the techniques for measuring thrust, exhaust velocity and ablated mass. These are discussed below.

Thrust

Since the thrust measurement is a vital performance parameter, a means of calibrating the thrust stand has been devised (Figs. 5 and 6). A physical pendulum of mass m is constructed to rotate about pivot point O, and impact the thruster, mass M, at a radius r. The impact point at r is designed to be the center of percussion about O so that no impact forces are transferred to the suspension structure. The pendulum and thrust stand are then considered a purely rotational system, with angular momentum about O being conserved.

The pendulum velocity immediately before and after impact is found by passing the focussed beam of a helium-neon laser through a grid of equi-spaced slits (50 line/inch Edmund Scientific Ronchi Ruling), and measuring the chopping frequency of the transmitted beam (Fig. 6). All other fixed characteristics of the pendulum such as the moment of inertia are known, so that the net momentum transferred to the thrust stand can be calculated. Simultaneously, the recoil momentum of the thrust stand is found using the position transducer (Fig. 7). Comparison of the two measurements yields a calibration constant that is applied to all subsequent thrust data obtained using the transducer method.

THRUST STAND CALIBRATOR SCHEMATIC

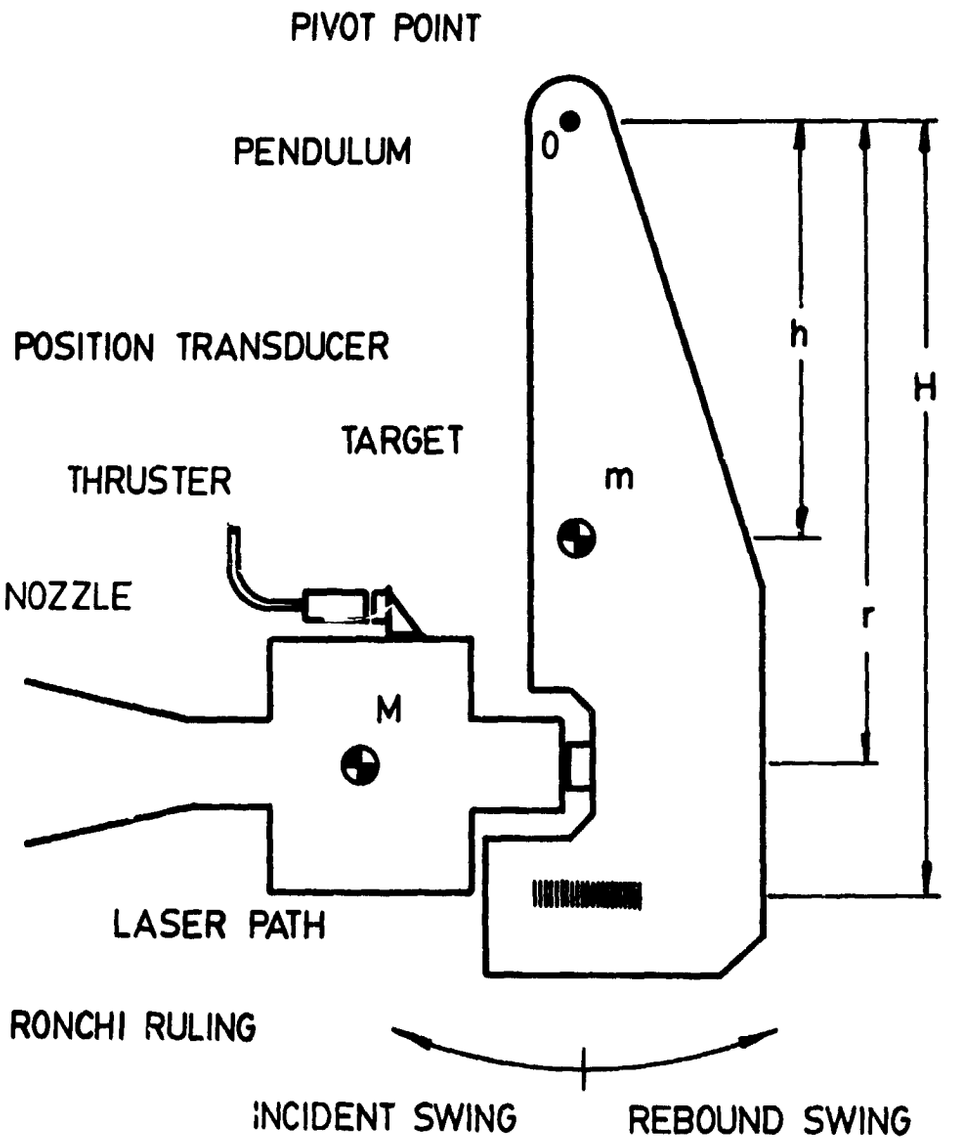

Figure 5

CALIBRATOR OPTICAL SCHEMATIC

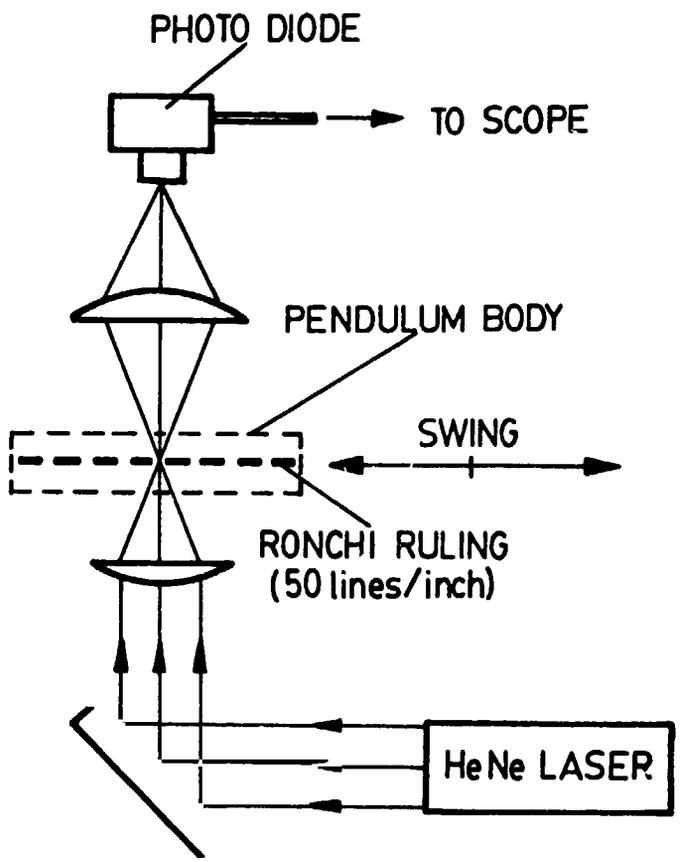

Figure 6

The design goal for the calibrator was to establish absolute confidence in the thrust measurement at the level of 5% or better. Some features of the calibration system are therefore noteworthy. All the basic physical characteristics of the pendulum, such as the mass m, moment of inertia I, and the various distances indicated in Figure 5, were measured to about 0.1% accuracy. Table I summarizes the relevant data. In Table I, T is the period of the free swinging pendulum, and Δx characterizes the Ronchi ruling grid pattern. The incident and rebound swing velocities, v_1 and v_2, are determined using the known Δx and by a linear least squares fit to the timing data presented by the rising and falling edges of the chopped laser response (Fig. 7). Overall, the pendulum calibrator has an inherent accuracy of $\pm$ 2%.

In order to mimic the recoil experienced by the thrust stand during a discharge, the pendulum was arranged to strike directly on and parallel to the thruster axis. As well, both the pendulum and thruster have hardened steel inserts at the contact point. Independent measurements indicate that this results in an impact time that is comparable to the duration of the discharge current pulse.

Throughout the course of the thruster experiments, calibration runs were made in order to monitor the stability and accuracy of the thrust measurements. The calculated recoil velocity differed from that measured by the position transducer by ±3% of the mean in the worst case. The average difference

THRUST STAND RECOIL AND CALIBRATOR RESPONSE

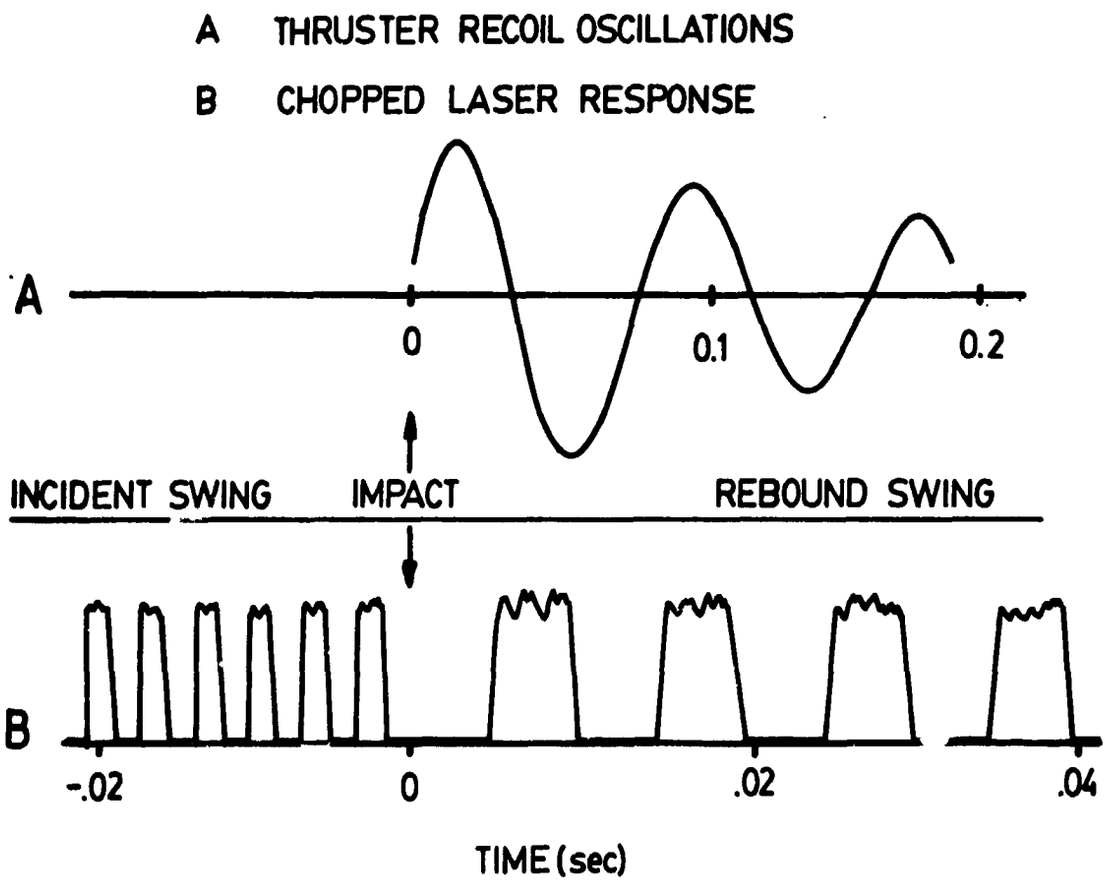

Figure 7

Table I. Pendulum Characteristics

$g = 980.1$ cm s^{-2}	± 0.10%
$h = 12.09$ cm	± 0.41%
$m = 404.81$ gm	± 0.05%
$T = 0.7875$ s	± 0.08%
$M = 2840$ gm	± 0.18%
$r = 15.24$ cm	± 0.28%
$H = 19.77$ cm	± 0.13%
$\Delta x = 254.0$ μm	± 0.8%

$$V_r = \frac{I}{MrH}(v_1 + v_2)$$

$$I = \left(\frac{T}{2\pi}\right)^2 mgh$$

$$v_1 = \Delta x/\Delta t_i$$

over several calibrations was only ±1.3%.

A further improvement in measuring the thruster recoil velocity was made by simply relocating the position transducer and target plate. Previously, experiments were performed by having the position transducer 'view' the recoil motion directly along the thrust axis (see Fig. 4 of Appendix A). In such a configuration, axial acoustic modes of the thrust stand produced a large amplitude, high frequency oscillation superimposed on the relatively slowly varying recoil signal. (See, for example, Figures 7 and 8 of Ref. [1].) However, by locating the transducer and target as shown in Figure 5, this acoustic 'noise' has been significantly reduced, allowing the recoil momentum to be determined to better than ± 4% (Fig. 2).

Exhaust Velocity

In order to measure nozzle exhaust velocity, three time-of-flight techniques were developed: ion saturation probes, piezoelectric stagnation pressure probes, and photodiode probes. The exhaust velocities measured using each of these techniques are in good agreement, and a detailed description of the individual methods is given in Appendix A.

The primary velocity diagnostic selected was the photodiode probe, since this type of probe produced the most reliable and reproducible time-of-arrival signals. Two identical probes were installed downstream of the nozzle and separated axially by 50.0 cm. By using two probes simultaneously and noting the difference in the arrival time of the exhaust plasma, the exhaust velocity is determined for each shot in the test series. As an example,

the time difference Δt and exhaust velocity for each shot in the long pulse (100 μsec) test series is shown in Table II. The major uncertainty here lies in extracting Δt from the individual photodiode traces. Each value for Δt is accurate to $< \pm 10\%$ so that, over the 10 shot test series, the average exhaust velocity is established to $\pm$ 5%. The tank pressure was kept at less than 0.003 torr in all cases, to prevent interference by the background gas with the exhaust gas.

Mass Loss Measurements

Ablation studies are carried out via a simple weighing procedure. All components exposed directly to the discharge plasma (cathode, capillary and nozzle) are weighed before and after each series of test shots. The improvement made here is to include the nozzle in the mass loss data, since the nozzle structure incorporates a polyethylene liner in the vicinity of the throat, where some ablation might still be expected.

All mass measurements are made using a Voland Model 220R balance having $\pm$ 0.1 mg resolution. However, experience has shown that the thruster assembly, disassembly and cleaning procedures introduce a total uncertainty of 1-2 mg. Therefore, capillary loss is typically accurate to $< \pm 5\%$ whereas the cathode and nozzle erosion data is less precise due to the smaller total mass loss.

The performance of the PET thruster was evaluated in four series of ten shots each. The capillary length and current pulse length were varied to permit the thruster to run in an unsteady or quasi-steady mode, depending on the number of

Table II. Exhaust Velocity Data For 100 μs Pulse Test Series

Shot No.	u_e(km/sec)	Δt(μs)
P165	-	-
166	27.8	18.0
167	27.9	17.9
168	27.6	18.1
169	24.8	20.2
170	25.4	19.7
171	26.2	19.1
172	25.6	19.5
173	28.1	17.8
174	29.1	17.2

$\langle u_e \rangle$ = 26.9 km/sec

σ = ± 1.47 km/sec ± 5.5%

Table III. Experimental Parameters for Polyethylene Propellant

Test Series	Capillary Energy, kJ	Pulse Length, μs	Capillary Length, cm	$\frac{ct_p}{2\ell}$
1.	1.80	15	15	0.4 Unsteady
2.	1.78	48	5.5	3.5 Quasi-steady
3.	1.89	48	4.5	4.3 Quasi-steady
4.	3.98	100	4.5	8.9 Quasi-steady

acoustic travel times $ct_p/2\ell$ during the current pulse. The four test series are summarized in Table III below.

After each series, the results of the ten shots were averaged. The performance results are summarized below in Table IV.

Based on the experimental results, the estimated precision of the results in Table IV is:

1. Recoil motion x(t); impulse bit is accurate to 5%.
2. Exhaust probe time-of-flight; exhaust velocity is accurate to 10%.
3. Current; accurate to 3%.
4. Voltage; accurate to 3%.
5. Mass loss Δm; accurate to 6%.

Summary

The probe measurements of exhaust velocity give results which are consistent with our understanding of the physics of the discharge. In the unsteady mode case (Series 1), the current impulsively heats the discharge plasma, which is then accelerated as the temperature decays. The measured exhaust velocities are 20-21 km/sec. The quasi-steady cases (Series 2-4) achieve nearly steady state conditions, and hence a higher mean sound speed for the duration of the pulse. The exhaust velocities are correspondingly higher: 26-28 km/sec. A discussion of the agreement of these measured velocities with a computational model is given in Appendix A.

The thrust to power ratio [N/kW] can be evaluated in the form

$$\frac{I}{\bar{P}}\,[N/kW] = \frac{\int T dt}{\int P dt} = \frac{\int T dt\,[N\text{-}s]}{E_D[kJ]}$$

Table IV. PET Thruster Performance With Polyethylene, 10 Shot Averages

Delivered energy, E_D	1.80 kJ	1.78 kJ	1.89 kJ	3.98 kJ
Maximum current, I_M	23 kA	17 kA	15 kA	15 kA
Pulse width, half max	15 μsec	48 μsec	48 μsec	100 μsec
Impulse bit, $\int Tdt$	.20 N-sec	.095 N-sec	.086 N-sec	.189 N-sec
Exhaust velocity:				
Pressure transducer	21 km/sec	28 km/sec	-	-
Photodiode probes	20 km/sec	26 km/sec	26 km/sec	27 km/sec
Capillary ablated mass	20 mg/shot	6.5 mg/shot	5.3 mg/shot	10.8 mg/shot
Electrode + nozzle ablated mass	N/A	N/A	0.9 mg/shot	2.0 mg/shot

The values of T/P for the test shots (Table IV) are shown below in Table V. The velocities shown are those measured by the velocity probes for the mass exhausted during the current pulse.

The thruster efficiency η_T is conventionally defined as

$$\eta_T = \frac{\text{exhaust kinetic energy}}{\text{energy delivered}} = \frac{1/2\ mu_e^2}{E_D}$$

Table V. Measured Thrust to Power Ratio for Polyethylene

	u_e(Probe)	T/P
1. Unsteady, 15 μsec pulse	21 km/sec	.10 N/kW
2. Quasi-steady 48 μsec pulse	27 km/sec	.053 N/kW
3. Quasi-steady 48 μsec pulse	26 km/sec	.046 N/kW
4. Quasi-steady 100 μsec pulse	27 km/sec	.048 N/kW

For a pulsed device, the exhaust kinetic energy is

$$1/2\ mu_e^2 = \int \frac{d}{dt}\left[\tfrac{1}{2}mu_e^2\right]dt$$

where the integral is continued past the end of the current pulse to account for the discharge afterglow, during which propellant evaporation decays to zero. Unfortunately the time dependence of m and u are not known, so that we must define the efficiency in terms of impulse bit as:

$$\eta_T = \frac{\left[\int T dt\right]^2}{2\Delta m E_D}$$

where Δm is the capillary ablated mass, and is used to define the specific impulse by

$$I_{sp} = \frac{\int T dt}{g \Delta m}$$

The data from Table V above can therefore be used to evaluate η_T and I_{sp} for Series 1-4, shown below in Table VI. It is important to note that we are basing the efficiency and I_{sp} in Table VI on the ablated mass and not on the measured exhaust velocity.

The specific impulse values in Table VI are about half of those indicated by the exhaust probe velocity measurements. This is primarily because the mass fraction ejected in the afterglow tail of the pulse has significantly lower velocity than the fraction ejected during the pulse. This is expected since the afterglow plasma is cooler.

Table VI. PET Thruster Efficiency and I_{sp} for Polyethylene at 2 kJ

		η_T	I_{sp}
1.	Unsteady 15 μsec pulse	.56	1000 sec
2.	Quasi-steady 48 μsec pulse	.39	1500 sec
3.	Quasi-steady 48 μsec pulse	.37	1600 sec
4.	Quasi-steady 100 μsec pulse	.42	1750 sec

Conclusions on PET Thruster Performance Measurements

A single-shot PET thruster has been built and tested on a thrust stand, giving repeatable reults over a series of shots. Exhaust velocities for polyethylene propellant vary from 20 to 27 km/sec, as measured by exhaust probes. These velocities are consistent with computational predictions of capillary conditions with an adiabatic expansion to high Mach number in a conical nozzle. Single pulse spcific impulse nd efficiency measurements, based on ablated mass, show a thruster efficiency of .37 to .56 in the 1000-1750 second range. We believe that an understanding of loss mechanisms in the discharge would lead to an improved design with a thruster efficiency of .70 to .80.

III. PET THRUSTER SYSTEM CONCEPTUAL DESIGN

In order to evaluate the PET thruster concept as a system, we have performed a conceptual design for a PET propulsion mission [2]. The two principal goals of the design are one, to design a practical propellant feed system and two, to estimate the system component masses.

The selected mission for the conceptual design is the orbit raising of a Space-Based Radar Satellite, a concept being developed by MIT Lincoln Laboratories (Fig. 8) [3]. The mission for this design is to raise the orbit of the SBR and change the orbital plane, following deployment by the Space Shuttle. The orbital altitude gain is from 150 n.m. circular to 600 n.m. circular, and the plane change is 4°. For the purposes of this study, the mission characteristic velocity is taken as ΔV = 1000 m/sec.

Several aspects of this SBR orbit-raising mission make it appropriate for the PET thruster conceptual design.

1. Solar panels and batteries on the SBR (Fig. 8) can supply 50 kW of power on a 200V DC bus. This power can be made available for orbit raising propulsion.

2. As much as 30 days can be allocated for the orbit raising, well within the capability of PET propulsion.

3. The proposed SBR initial orbit (150 n.m. circular, 57° inclination) is difficult to reach by the Shuttle, placing a premium on initial mass. The low propellant mass of electric propulsion is therefore attractive.

GTD

SBR SATELLITE / PET PROPULSION CONFIGURATION

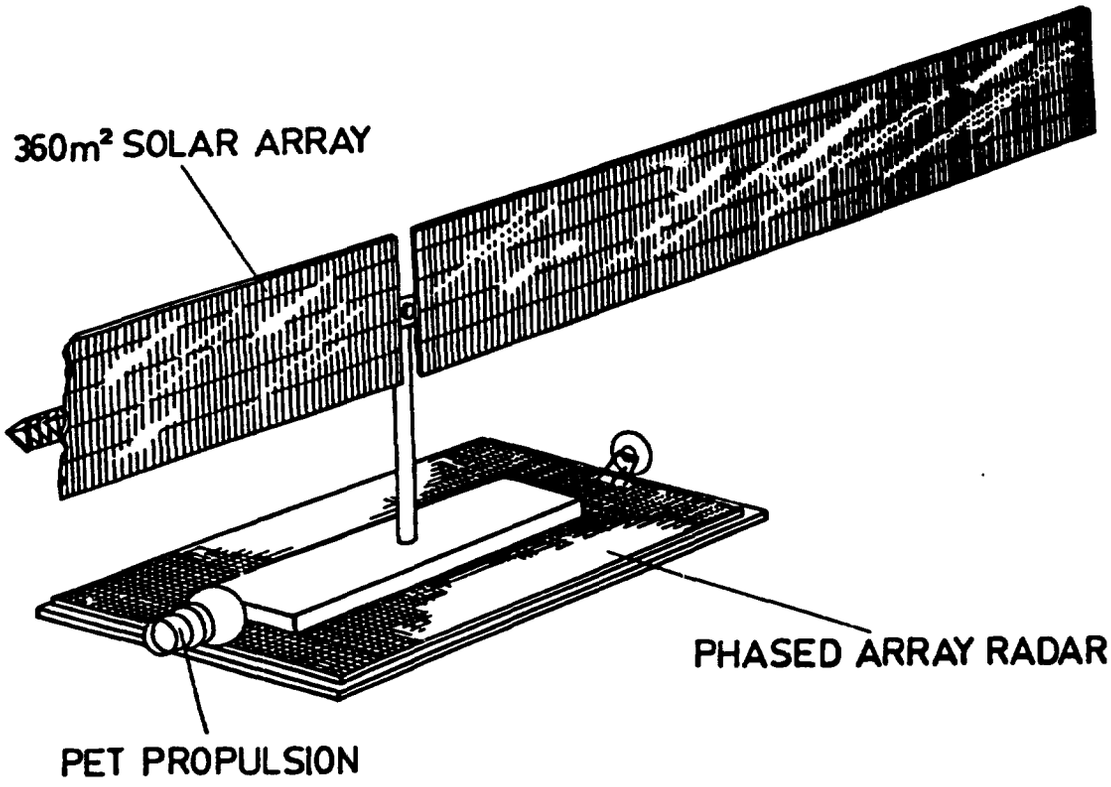

Figure 8

4. The inherently low acceleration of a PET-propelled SBR system, approximately 10^{-4} g, is consistent with the structural requirements of a large deployed solar array.

5. The high specific impulse and pulsed operational capability of PET propulsion would be attractive for station-keeping and precision attitude control during radar operations, although this aspect was not included in this design.

6. PET propellants can be benign chemically, an important consideration with respect to contamination of solar panels by propulsion system exhaust.

Mission Parameters

A Lincoln Laboratory estimate of the mass of the SBR satellite with chemical propulsion is 9800 kg, of which 2800 kg is propellant. These values are consistent with a characteristic velocity of ΔV = 1000 m/sec and a specific impulse of 300 seconds. By comparison, the specific impulse of PET is considerably higher, resulting in increased trip time and reduced propellant mass for the orbit-raising mission.

The calculation of trip time for the SBR satellite is performed for the simple case of constant specific impulse, thrust, and efficiency. The SBR satellite has sufficient battery capacity so that thrust can be maintained during solar eclipse. Hence, trip time and thrust time are assumed equal. The thrust is given by

$$T = \frac{2\eta_c \eta_T P}{u_e}$$

where η_c and η_T are the power conditioning and PET thruster

efficiencies, P is available bus power, and u_e is exhaust velocity. For the simple case of constant T and u_e, the integration of T = m(t)a gives a trip time of Δt of:

$$\Delta t[\text{sec}] = \frac{1/2\ m_f u_e^2}{\eta_c \eta_T P}\left[e^{\Delta v/u_e} - 1\right]$$

The trip time and required initial mass m_i are calculated for the values given below in Table VII. The calculation of the PET propulsion system dry mass of 400 kg is discussed in detail below.

Table VII. Space Based Radar Trip Time Parameters

Final mass, m_f (SBR, 7000 kg; PET propulsion, 400 kg)	7400 kg
Delivered Power, $P_T = \eta_c P$	40 kW
Thruster efficiency, η_T	0.5, 0.6, 0.7
Mission ΔV	1 km/sec
Specific impulse	$400 < I_{sp} < 1600$ sec

The trip time for the ΔV = 1000 m/sec orbit transfer is plotted in Fig. 9 for the parameters in Table VII. The thruster efficiency range of .50 to .70 represents the expected operating regime of the PET thruster. Trip time in Fig. 9 decreases monotonically with decreasing I_{sp}, reaching 7-9 days for continuous thrust at 400 seconds, for an initial mass of 9500 kg. At higher specific impulse the initial mass is reduced, reaching 8250 kg at 1000 seconds. At still higher I_{sp} the initial mass decreases further but the trip time increases rapidly. A design point is selected giving Δt = 15 days at 1000 seconds and .70 efficiency (Fig. 9). Recent experimental results, discussed above, indicate that this design point is a realistic one for a PET propulsion system. A summary of the design point conditions is shown below in Table VIII.

Propulsion System Design

Experimental work to date on the Pulsed Electrothermal (PET) thruster has been limited to ablative-wall versions of the device, using polyethylene or Teflon propellant, and described previously [1,4,5]. For the SBR orbit-raising mission the thruster must be non-ablative to meet the required system life of 15 days. Furthermore, a liquid propellant is required so that a central tank system can be used to supply several thrusters. Since the thrusters are low mass and compact, the use of liquid propellant permits several tens of thrusters to be installed, although only two are operated at any given time. This approach greatly increases system reliability with a low mass penalty.

TRIP TIME vs INITIAL MASS

SBR SATELLITE/PET PROPULSION

TRIP TIME, $\Delta V = 1$ km/sec

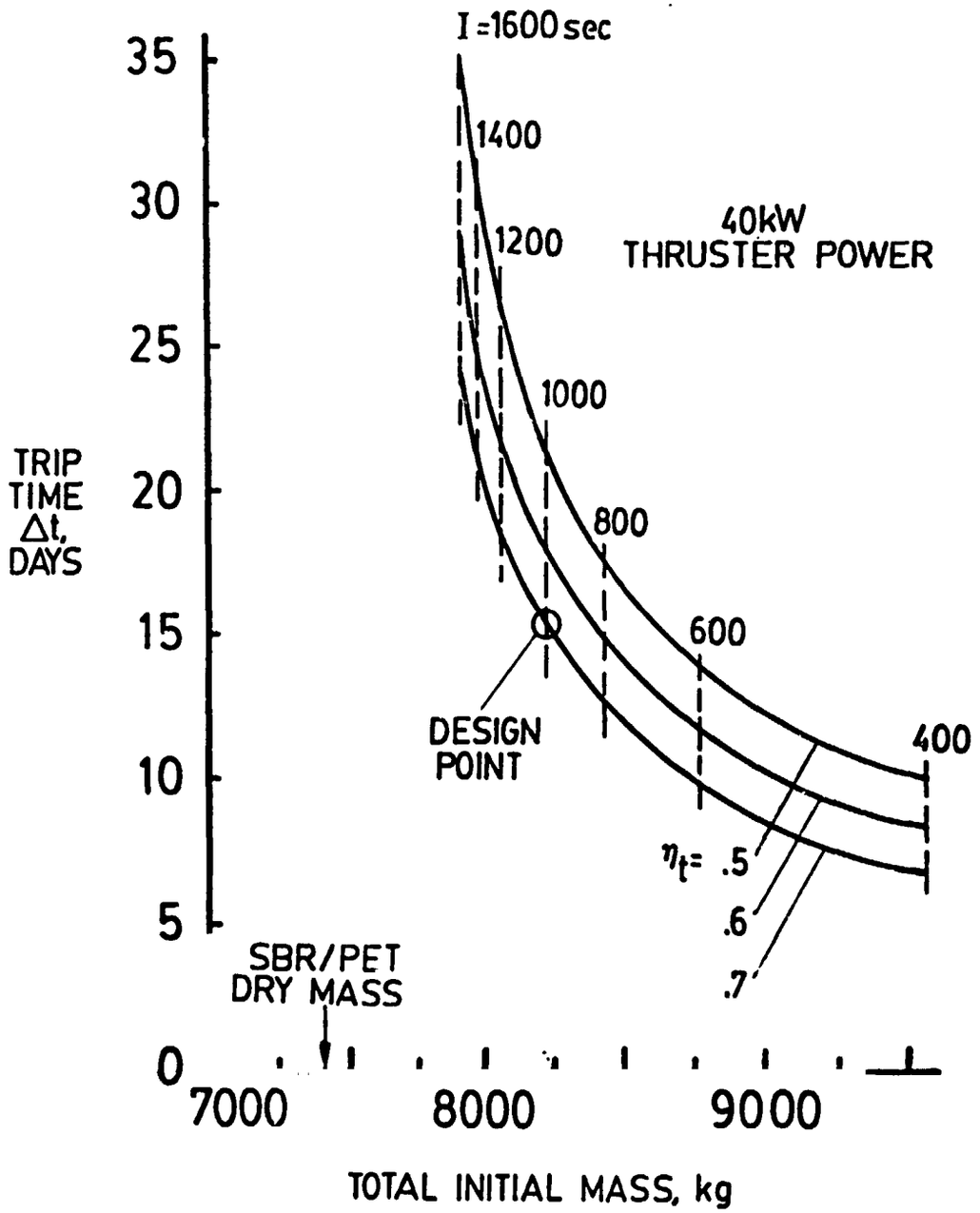

Figure 9

Table VIII. Design Point Parameters for SBR Mission, $\Delta V = .1$ km/sec

Initial mass, m_i	8250 kg
Final mass, m_t	7400 kg
Propellant mass, m_p	850 kg
Thruster efficiency, η_T	0.70
System efficiency, $\eta = \eta_c \eta_T$	0.62
Specific impulse, I_{sp}	1000 sec
Input power, P	45 kW
Thrust, T	5.6 N
Trip time, Δt	15 days

Water (mol. wt. 18) is the liquid of choice for the propellant. The advantages of water are:

1. Easily storable.
2. Existing space-qualified flow hardware.
3. Simple blowdown injection.
4. Propellant chemistry matched to mission.
5. Low expected spacecraft/environmental contamination.
6. Non-reactive, non-toxic.
7. Convenient vapor pressure for no-switch operation.
8. Known thermodynamic properties.

Items 4 and 7 in the above list require further comment. First (item 4), the propellant chemistry of water is well matched to the SBR mission, which is designed for 1000 seconds specific impulse. This specific impulse can be achieved by water at a temperature below 1 eV (11,6000 K), as required for non-ablative thruster operation. Unsteady heat transfer calculations for ten microsecond, 1 eV discharges show that the working temperature will not be exceeded for available insulator, electrode and nozzle materials.

Numerical calculations of the capillary performance with water have been performed (Fig. 10), and water can be seen to be similar to the behavior of polyethylene in terms of pressure, temperature and sound speed. All curves in Figure 10 were calculated using the experimental power pulse shown at the bottom of Figure 1.

Second (item 7), the PET thruster is designed to fire at a rate of several hundred pulses per second. This is accomplished without the aid of a switch or trigger circuit, by permitting Paschen breakdown through the water vapor surrounding the injected liquid. This mode of operation has been experimentally demonstrated recently at GT-Devices at breakdown voltages of several kilovolts.

The basic elements of the PET thruster operating with water are shown in Figures 11-14. In the schematic of the operating system (Fig. 11), a high voltage DC charging supply, powered from the SBR satellite 200V DC bus, charges a capacitive pulse forming network. Simultaneously, liquid water flows into the discharge chamber through the central electrode. The flow rate and the charge rate are roughly timed, so that the breakdown voltage is reached when the leading edge of the injected water is just reaching the throat of the supersonic nozzle. The PFN energy is discharged in a few tens of microseconds, and the heated water expands through the equilibrium flow nozzle. The cycle then repeats. Because no pulsed water valve is in the system, the pulse rate can be several hundred pulses per second.

GTD

COMPUTED CAPILLARY PERFORMANCE

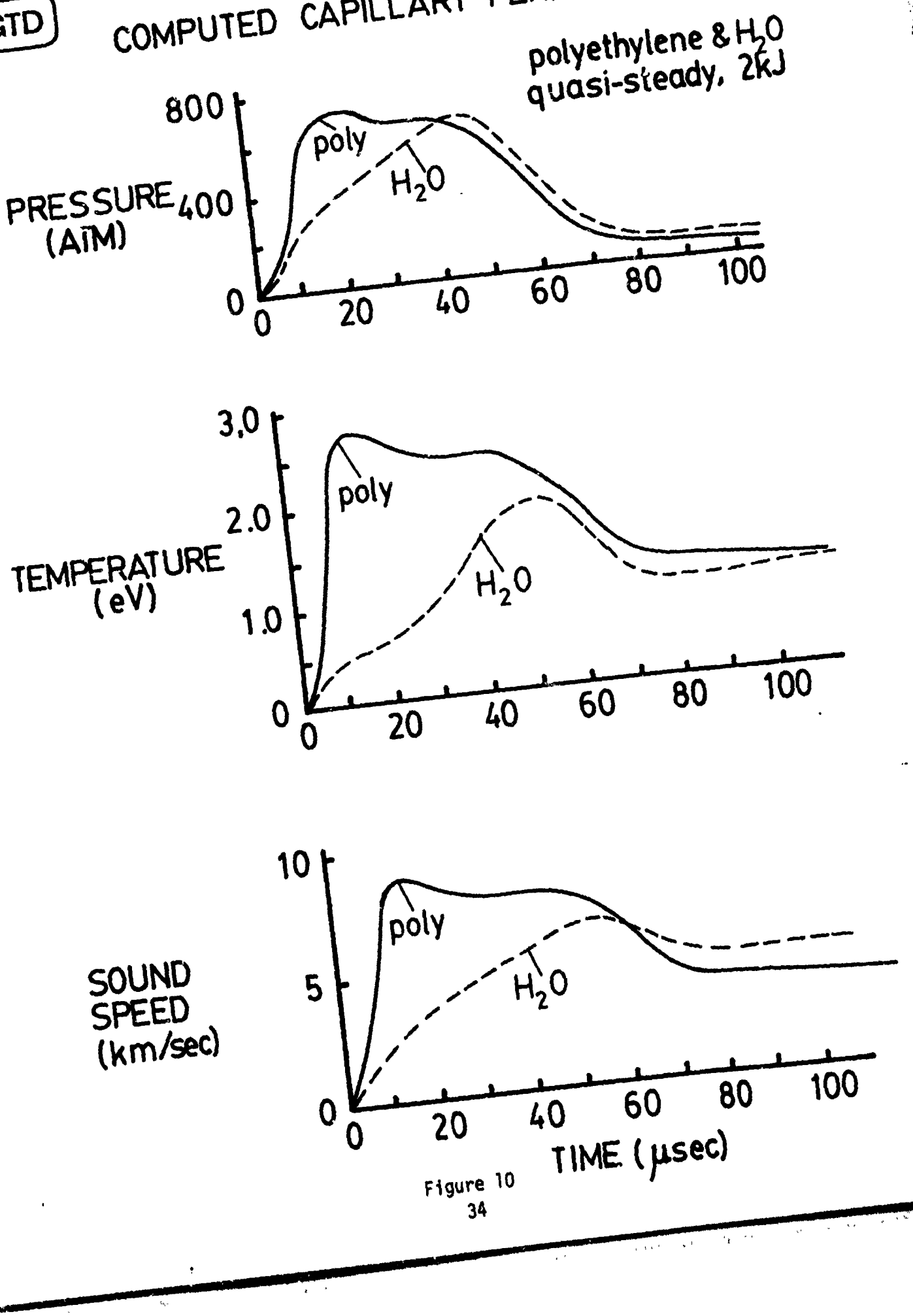

Figure 10

GTD

20kW PET THRUSTER SCHEMATIC

water propellant
100 J/pulse
200 pulses/sec

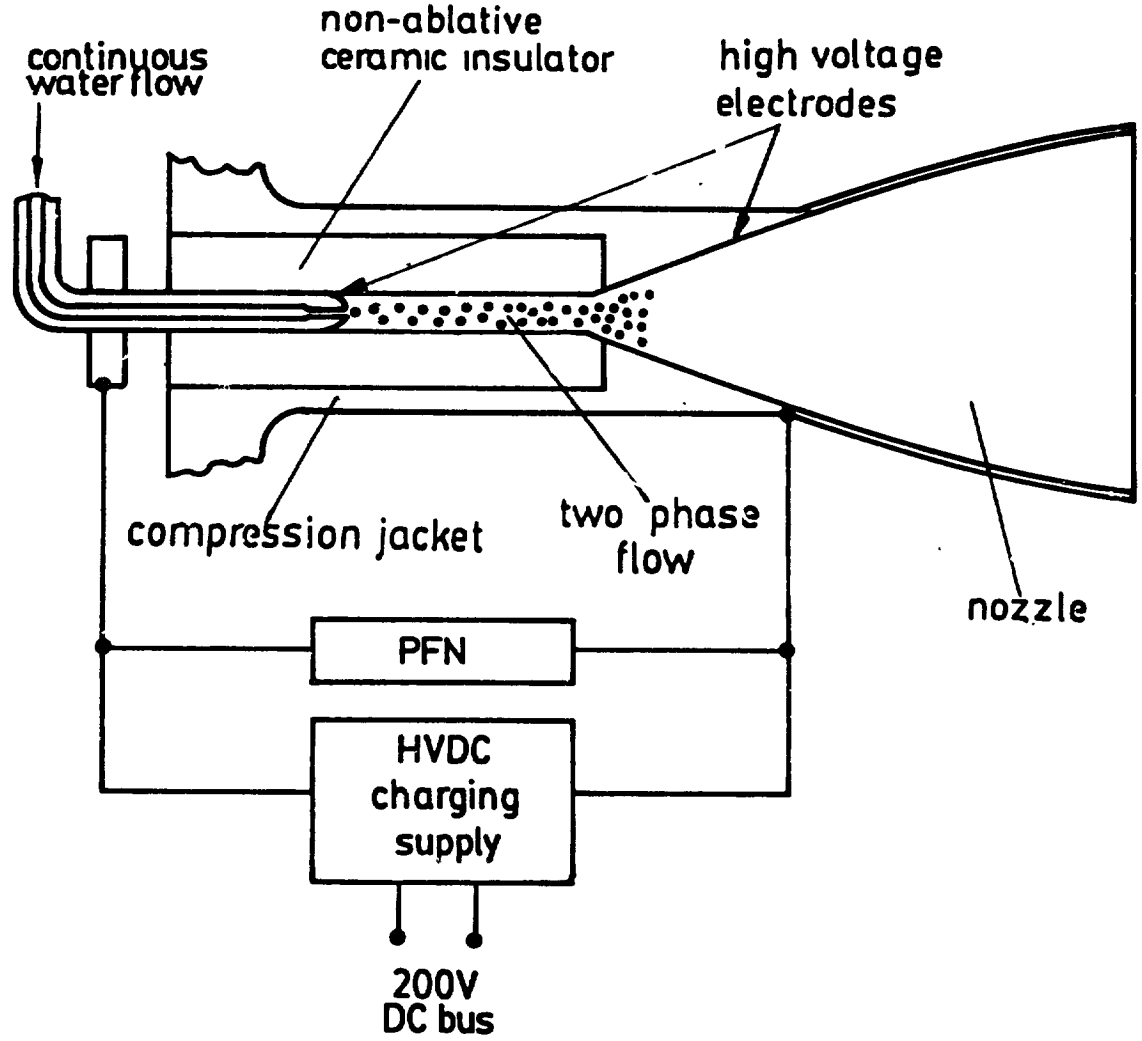

Figure 11

The water-injected PET thruster requires a non-ablative insulator capable of withstanding thermal and mechanical shock, and the high heat transfer conditions of the discharge. The best candidates for this insulator are high-performance ceramics. Hot-pressed silicon nitride, for example, has been used for gas turbine wheels and diesel pistons [6], and is one of several good candidates for the PET thruster application. Advantage can be taken of the very high compressive strength of ceramics by shrinking a steel compression jacket (Fig. 11) around the insulator, as has been done in similar applications [7].

A schematic of the PET thruster module with a radiator is shown in Fig. 12. Two modules are operated in parallel in the present design. A high voltage insulator is used to isolate the water feed system from the high voltage current pulse. This insulator takes advantage of the high dielectric strength and resistivity of water.

The mass of the SBR 40 kW PET propulsion system is estimated from the component masses of space qualified hardware. We have adapted a design similar to that for the Viking 75 Orbiter spacecraft, which carried a helium-pressurized chemical bipropellant system for trajectory correction and maneuvering in orbit around Mars [8]. Total Viking Orbiter propellant mass is 1426 kg, and the mass of propellant and pressurant tanks for the 850 kg propellant PET system is scaled down proportionately. This mass estimate is conservative, since the VO'75 design incorporates two tanks with an internal pressure of 8 atm,

GTD

PET THRUSTER MODULE

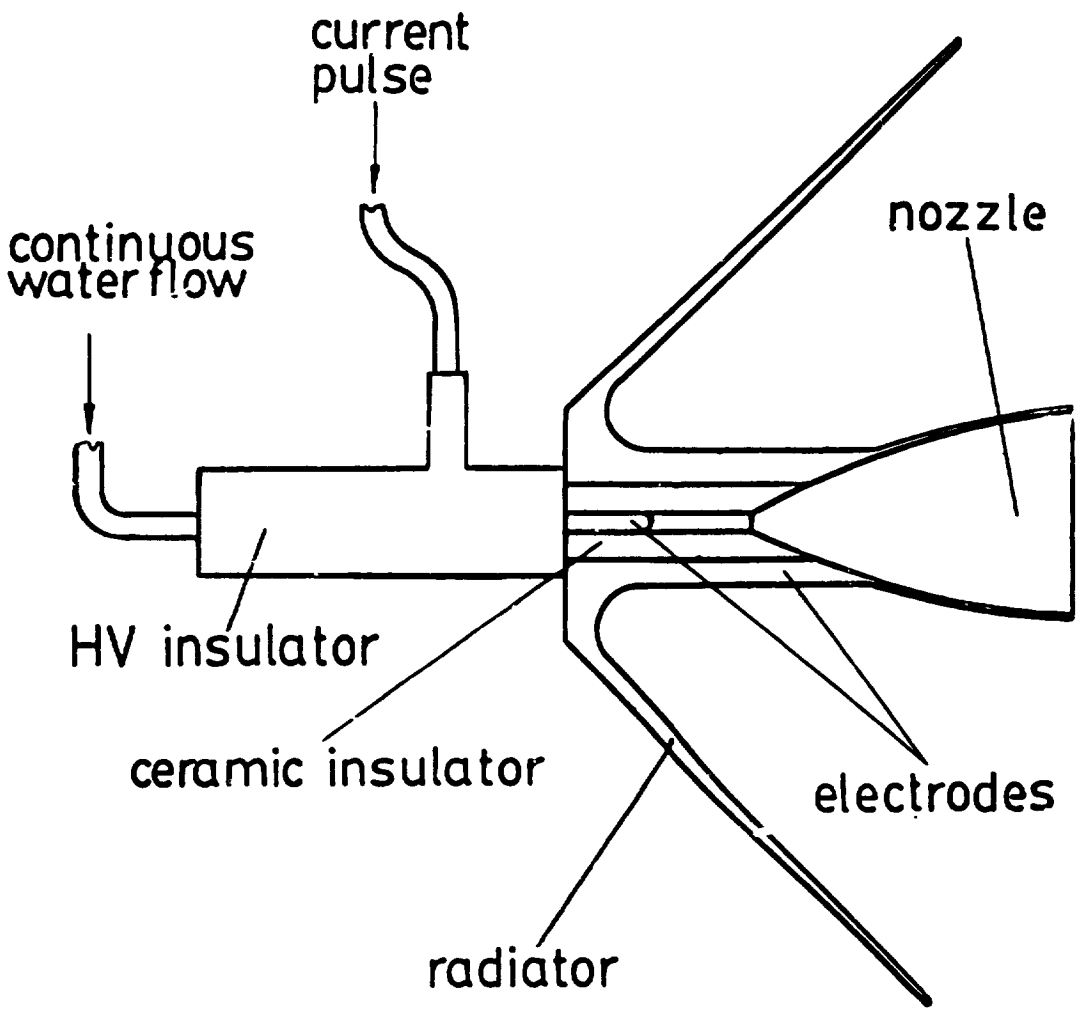

Figure 12

whereas the PET system requires one tank with an internal pressure of 4 atm.

The SBR 40 kW PET design achieves redundancy by incorporating 20 PET thrusters with propellant shutoff valves and electrical connect switches. Two 20 kW thrusters are in operation at any given time, each driven by an independent 100 J pulse forming network (Fig. 13).

The flow and electrical schematics are shown in Fig. 14. The pressurant helium for the propellant tank is regulated to 4 atm, and the pressurized water to each thruster flows through a filter, a shutoff valve, and the injection orifice to the discharge chamber. Back flow caused by chamber discharge pressure is not expected to be significant, due to the small size of the injection orifice (<0.3 mm dia), short duration of the pulse (10 μsec), and low density of the mass in the discharge chamber (.005 g/cm^3). Mass estimates for propellant flow hardware are based on the V0'75 system (19 items, total mass 12 kg) [8] and on mass values supplied by manufacturers for solenoid valves and filters [9], cartridge-actuated valves [10], and high voltage switches [11].

Each thruster is connected to one of two 100 J pulse forming networks through a latching connect switch. Switch operation is only permitted with the PFN at zero voltage to prevent electrode arcing. In addition, each capacitor and inductor in the PFN are connected via DPDT latching switches, to allow removal of a failed capacitor from the system. Capacitor mass is based on a conservative 12 J/kg, which should permit a design life of 10^9

GTD

40kW PET PROPULSION MODULE

propellant 860 KG
dry mass 400 KG
thrust 6 N

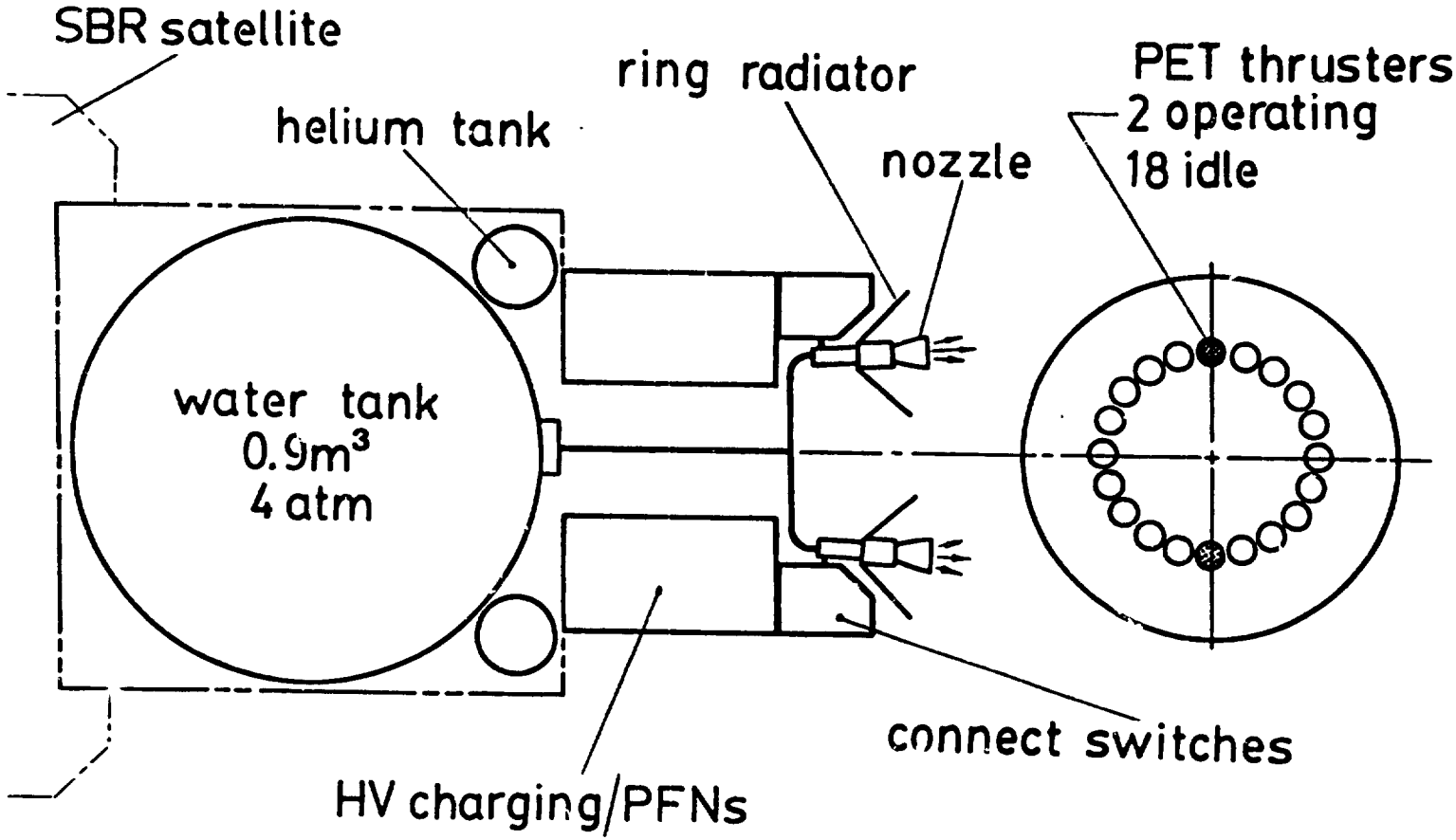

Figure 13

GTD

20kW PET PROPULSION SCHEMATIC

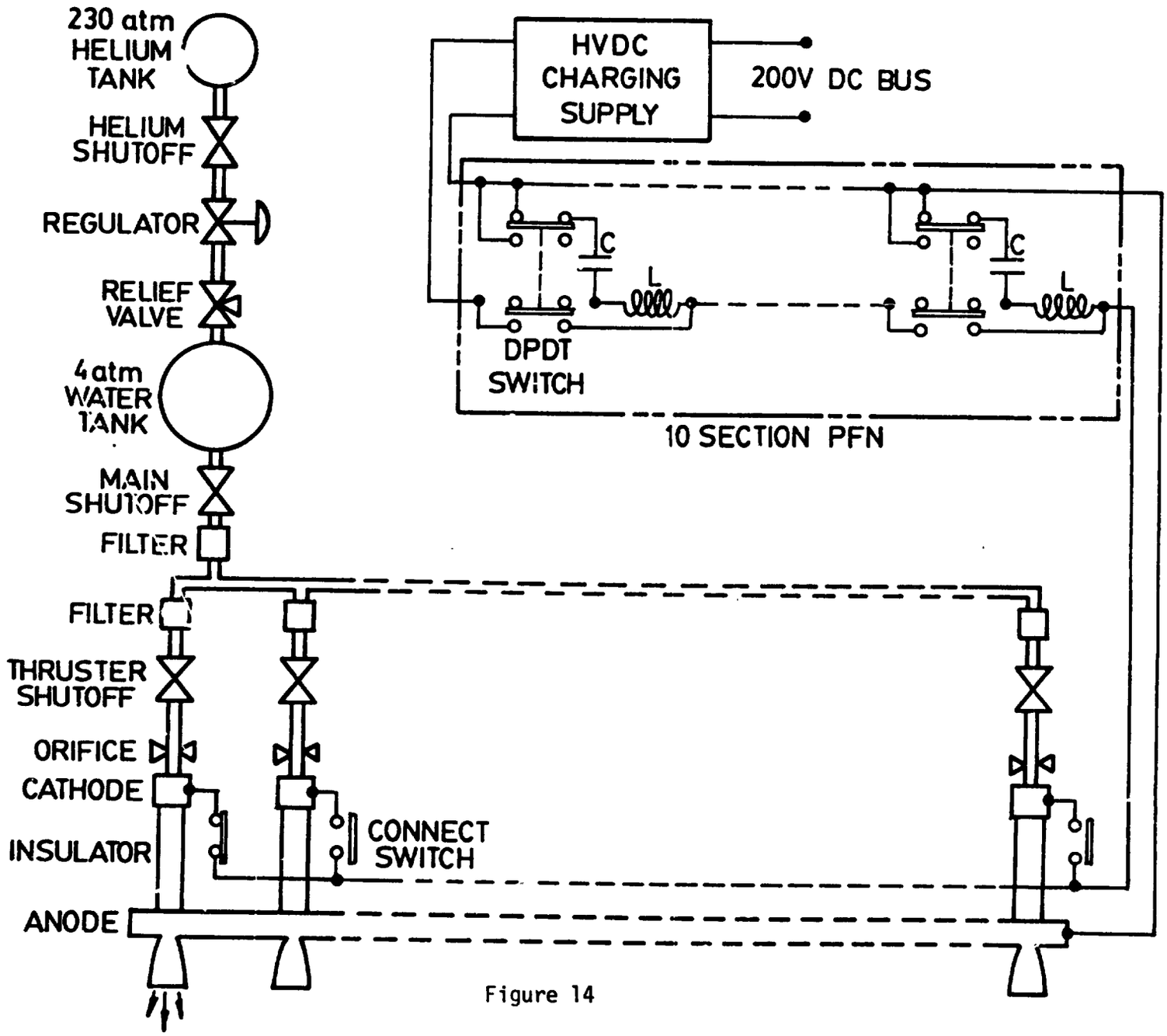

Figure 14

cycles in a non-reversing application [12]. This value can be compared with the capacitor bank used for the Pulsed Plasma Teflon thruster which operates at 64 J/kg [13]. This conservative 12 J/kg rating is feasible because of the low energy per pulse of the PET system.

The mass of the power conditioning and logic circuits is an extrapolation of series resonant charging technology. The SBR DC bus voltage is 200V, and the discharge breakdown voltage is 4 kV. It is estimated, from experience with Pulsed Plasma thruster technology, that an 89% efficient, 20 kW power conditioning and logic module can be built at a specific mass of 2.5 kg/kW [14]. The power conditioner is thus the most massive component in the system.

The thruster modules are designed for containment of the 10^3 atm discharge pressure in a 1 cm^3 capillary volume. They are conservatively estimated to have a mass of 1 kg each, including nozzles and insulators. The thrusters are mounted on a common radiator ring designed to radiate a total of 4 kW from 2 thrusters at a mean temperature of 540°C. The radiator material is assumed to be a copper-stainless steel sandwich for high temperature strength, formed into a dished donut (Fig. 13).

The mass of the structure is estimated from the VO'75 design, for which structure mass was 11% of the total non-structural non-fluid mass [8]. A figure of 11% is therefore adopted for this design.

The component masses for the SBR 40 kW PET propulsion system are summarized below in Table IX. The predicted specific mass of

Table IX. Component Masses, SBR 40 kW PET Propulsion

	Mass, kg
A. Propellant Handling	
Water tank, 860 kg, 4 atm	61
Water holdup	10
Helium pressurant tank, 230 atm	21
Helium pressurant	3
Main shutoff, regulator, relief, main filter	6
Thruster filters, 20	10
Thruster shutoff valves, 20	10
Propellant lines	10
Subtotal	131 kg
B. Power Conditioning	
Series resonant DC-DC charger, 2 @ 20 kW, 5 kV	100
Capacitors, 20 @ 10 J	16
Inductors, wiring, insulation	10
Thruster connect latching relays, 20	30
PFN connect switches latching DPPT, 20	25
Subtotal	181 kg
C. Thrusters	
Modules with nozzles, 20	20
Radiator ring, 20 thrusters	25
Subtotal	45 kg
D. Structure, 11% of non-fluid mass	40 kg
Total mass:	400 kg
Specific mass:	α = 10 kg/kW

the entire system is α = 10 kg/kW.

If more thruster redundancy is required for longer system life, 20 kW thruster modules can be added at a total system mass penalty of 7 kG per thruster. Doubling the number of thrusters from 20 to 40, for example, would increase the total mass from 400 kg to 540 kg and raise the system specific mass to 13.5 kg/kW.

Of the major research issues which need to be addressed for PET propulsion thruster efficiency is the only one which can have a large impact on the design. The remaining issues, such as peak discharge temperature and pressure, water injection nozzle design, and insulator and capacitor life, will have a relatively small effect. If the present experimental efficiency of .50 cannot be improved to the assumed value of .70, the trip time would increase from 15 days to 24 days, but there would be no increase in the initial mass.

IV. CONCLUSIONS

We have performed definitive and accurate experiments to characterize the performance of a single-shot, ablative Pulsed Electrothermal (PET) thruster. The data show that the thruster efficiency range is .37 to .56 at 1000 to 1750 seconds. In our opinion, the efficiency can be raised to .70 through design improvements.

We have also proposed a non-ablative PET thruster concept, using water propellant. Numerical calculations show that this thruster would have similar performance to the ablative thruster, with significant system advantages in redundancy, reliability, and thruster lifetime. Based on these results, a repetitively operated, non-ablative PET thruster can now be designed and tested, with a performance goal of .70 efficiency at 1000 seconds. We expect that this device would prove superior to other propulsion devices operating at this specific impulse.

V. ACKNOWLEDGEMENTS

We would like to acknowledge many useful discussions with F. Terdan and S. Wang of NASA Lewis Research Center.

We are also indebted to R. Frye and M. Brasher of NASA Lewis and to K. Clark of RCA Astro-Electronics for many helpful suggestions.

This work was supported in part by NASA Lewis and in part by GT-Devices.

VI. REFERENCES

1. Burton, R. L., Goldstein, S. A., Hilko, B. K., Tidman, D. A., and Winsor, N. K., "Investigation of a Pulsed Electrothermal Thruster", Final Report No. NASA CR-168266, NASA-LEWIS Research Center, October 1, 1983.

2. Burton, R. L., Goldstein, S. A., Hilko, B. K., Tidman, D. A., and Winsor N. K., "Proposed System Design for a 20 kW Pulsed Electrothermal Thruster", AIAA Paper No. 84-1387, AIAA/SAE/ASME 20th Joint Propulsion Conference Cincinnati, OH, June 11-13, 1984.

3. Vitto, V., and Pope, M. D., "Spacecraft Design Overview", MIT Lincoln Laboratory Program Review, 29-30 November 1983.

4. Burton, R. L., Goldstein, S. A., Tidman, D. A., and Winsor, N. K., "Theory of the Pulsed Electrothermal Thruster", AIAA Paper No. 82-1952, AIAA/JSASS/DGLR 16th International Electric Propulsion Conference, New Orleans, November 17-19, 1982.

5 Burton, R. L., Goldstein, S. A., Hilko, B. K., Tidman, D. A., and Winsor, N. K., "Experimental Investigation of the Pulsed Electrothermal (PET) Thrust[illegible]", AIAA Paper No. 84-1386, AIAA/SAE/ASME 20th Joint Propulsion Conference Cincinnati, OH, June 11-13, 1984.

6 Govila, R. K., "Material Parameters for Life Prediction in Ceramics", in Army Materials Technology Conference, Proc. (6th, 1979, Orcas Island, Washington), "Ceramics for High-Performance Applications, III, Reliability", Lenoe, E. M, et al. [eds], Plenum Press, New York, 1983, pp. 535-567.

7. Iton, T., Miyamoto, T., and Takano, N., "Permanent Power Fuse Self-Recovering Current Limiting Device", IEEE Summer Power Meeting and EHV Conference, Los Angeles, July 12-17, 1970.

8. Vote, F. C., and Schatz, W. J., "Development of the Propulsion Subsystem for the Viking 75 Orbiter", AIAA Paper No. 73-1208, AIAA/SAE 9th Propulsion Conference, Las Vegas, November 5-7, 1973.

9. Vacco Industries, South El Monte, California.

10. Pyronetics Devices, Inc., Denver, Colorado.

11. Ross Engineering Corporation, Campbell, California.

12. Maxwell Laboratories, Inc., San Diego, California.

13. Palumbo, D., Begun, M., and Levy, G., "Millipound Pulsed Plasma Thruster Electronic Subsystem", AFRPL TR-82-098, Air Force Rocket Propulsion Laboratory Final Report, December 1982.

14. Frye, R., NASA-Lewis Research Center. Private Communication.

AIAA'84

AIAA-84-1386
Experimental Investigation of the Pulsed Electrothermal (Pet) Thruster

R. L. Burton, S. A. Goldstein,
B. K. Hilko, D. A. Tidman and
N. K. Winsor, GT - Devices, Inc.,
Alexandria, VA

AIAA/SAE/ASME
20th Joint Propulsion Conference
June 11-13, 1984/Cincinnati, Ohio

EXPERIMENTAL INVESTIGATION OF THE PULSED ELECTROTHERMAL (PET) THRUSTER

R. L. Burton*, S. A. Goldstein, B. K. Hilko,
D. A. Tidman and N. K. Winsor

GT-Devices, Inc.
Alexandria, VA 22312

Abstract

Exhaust velocity, thrust, and mass consumption measurements are performed on a Pulsed Electrothermal (PET) thruster using polyethylene propellant. The data verify theoretical predictions of equilibrium flow in the supersonic nozzle, resulting in nearly complete recovery of the energy of ionization. The thruster is tested in an acoustically unsteady mode (15 μsec current pulse) and in an acoustically quasi-steady mode (48 and 100 μsec current pulses) at 2 and 4 kJ. The exhaust velocity of the propellant mass exiting during the current pulse is measured with three types of time-of-flight probes, and the impulse bit is measured on a thrust stand. The measured thrust to power ratio is T/P = 0.10 N/kW at 21 km/sec in the unsteady mode and T/P = 0.05 N/kW at 27 km/sec in the quasi-steady mode. The discharge pressure, temperature, and sound speed predicted by a computational model are consistent with the measured thrust and discharge resistance. Propellant consumption is determined by weighing the loss for 10 shots at fixed conditions. The total measured consumption is in excellent agreement with that given by the model, which predicts that about 2/3 of the mass is ablated during the current pulse and about 1/3 at later times. The computed sound speed for polyethylene is 9 km/sec, indicating that the exhaust plasma (27 km/sec) is highly supersonic. The thruster efficiency varies from .37 to .56 for 1000-1750 seconds specific impulse.

Introduction

In a previous paper [1] we have discussed the theory of the Pulsed Electrothermal (PET) thruster, a device which in principle can operate with 70% efficiency at a specific impulse of 1000 seconds and higher. This level of performance would be particularly attractive for orbit raising of large satellites and other near-earth missions, which cannot be easily accomplished by chemical propulsion. We have recently completed a series of experiments to measure the single-shot performance of a PET thruster on a thrust stand. These experiments confirm that our theoretical understanding of the pulsed electrothermal approach is essentially correct, and that the PET thruster is potentially capable of significant performance improvements over steady-state devices.

In its simplest form, the PET thruster (Fig. 1) consists of a long, thin, discharge channel, closed on one end and coupled on the other end to a conventional supersonic nozzle. The current flows from the anode located in the nozzle downstream of the throat, to the cathode located in the closed end. The pressure chamber inner wall is lined with an easily ablated, low molecular weight material such as polyethylene or Teflon. The pressure chamber is a high strength dielectric, capable of withstanding plasma pressure pulses up to several thousand atmospheres. The high pressure develops a jet of high velocity plasma from the nozzle, which provides rocket thrust.

The electrical energy store (Fig. 1) consists of a high voltage capacitive pulse forming network, capable of storing a few kilojoules at several kilovolts. The impedance of this source is matched to the discharge resistance R for efficient coupling. The switch is an ignitron with resistance $R_s \ll R$, so that over 90% of the stored energy is transferred to the discharge in a single pulse. The width of the current pulse is 15-100 μsec, with a peak in the 15-22kA range. Terminal voltage is 2-3 kV, giving a peak power dissipation on the order of 50 MW.

We discuss results from two PET thruster operating modes in this paper. The mode is determined by comparing the length of the current pulse, t_p, to the two-way longitudinal acoustic time in the capillary, $2\ell/c$. In the short pulse or unsteady mode, $t_p c/2\ell < 1$, and steady flow is not achieved through the nozzle. In the long pulse or quasi-steady mode, $t_p c/2\ell \gg 1$, and steady flow is achieved during the high current portion of the pulse. The three current waveforms tested, with pulse lengths of 15, 48 and 100 μsec, are shown in Fig. 2.

Physics of Operation

For a PET thruster operating with an ablative liner at millitorr background pressures, the initial voltage breakdown occurs as a surface flashover, mostly in carbon residue along the wall. Within several microseconds the current, power input, pressure and temperature all rise to their peak values, and wall material begins to boil off, filling the capillary. The pressure, on the order of 10^3 atmospheres, generates a mass flow through the nozzle, which for constant power input balances the mass evaporating off the wall. When the

*Member AIAA

current falls at the end of the pulse, power input falls rapidly. The remaining plasma energy causes an afterglow of continued wall ablation at low pressure for many microseconds, and this afterglow increases the total mass ablated during the pulse.

Because the currents in the discharge are typically 20kA, the magnetic pressure is only a few percent of the gasdynamic pressure of 10^3 atm. This places the PET thruster firmly in the electrothermal thruster category, and justifies ignoring magnetic effects on the plasma acceleration process.

A second effect which may be ignored is the compression of the plastic wall material by the discharge pressure. For example, the volume compressibility of high density polyethylene at 10^3 atm is .98, so that this factor reduces the electrical resistance by only 6%. Since the PFN consequently drives the current to a slightly higher value, the power input I^2R is nearly constant.

Nozzle Processes

Without an equilibrium flow nozzle, the plasma exhaust would be highly ionized, resulting in high frozen flow losses. As shown below in the experimental results, however, the ionization energy is recovered by three-body recombination in the nozzle. This rate scales as [2]:

$$\nu_3 \sim n_e^2 T_e^{-4.5}$$

where n_e and T_e are the electron density and temperature. We compare the collisional recombination time $1/\nu_3$, to the particle flow time through the nozzle, using conditions at the exit plane where the smallest value of ν_3 occurs. We find that the condition $\nu_3 \ell / \langle u_e \rangle >> 1$ is easily satisfied [1], so that recombination collisions are frequent. The flow expansion process therefore remains close to Saha equilibrium, and because of the high expansion ratio the temperature drops to ~0.5 eV and most of the ionization energy is recovered.

Thrust Efficiency

The high thrust efficiency of the PET thruster is primarily attributed to two factors: efficient transfer of electrical energy to plasma enthalpy, and efficient conversion of plasma enthalpy to streaming velocity in the nozzle. The first factor is a result of the high radiation absorption coefficient of the black high density polyethylene propellant, and the high view factor of the capillary walls for the discharge black body radiation. The second factor is due to the ability of the high area ratio, high Reynolds number nozzle to achieve nearly equilibrium, adiabatic flow.

For the nozzle expansion of polyethylene (CH_2) plasma from To = 2 eV to T=0.5 eV, the effective ratio of specific heats is about γ = 1.2, so the exit Mach number is 5.5 and the area ratio is 220. The pressure drops from 10^3 atm to .2 atm. From the Saha equation we can estimate conditions at the exit plane. At low temperatures the degree of ionization is:

$$\alpha \simeq 3.11 \times 10^4 p^{-1/2} T_{eV}^{5/4} e^{-\varepsilon/2T_{eV}}$$

For an ionization potential ε = 11.2 eV for carbon, $\alpha \simeq 10^{-3}$, so that the average loss of ionization energy is .01 eV/ion, and can be neglected.

Dissociation is more significant. The dissociation energy of the C-H bond is ε_d = 4.5 eV [3], and the Saha equation predicts a dissociation fraction $\beta \simeq .7$, corresponding to a loss of energy in the exhaust stream of 2.0 eV/ion. Adding to the dissociation loss a thermal component of 5/2 T_e gives an approximate enthalpy in the exit plane of 3.3 eV/ion. For the assumed initial conditions the stagnation enthalpy is 12.6 eV/ion, so the ideal thruster efficiency is:

$$(\eta_T)_{ideal} = 1 - \frac{3.3}{12.6} = .74$$

The specific impulse for this example is given by $I_{sp} = [2(H_o - H_e)]^{1/2}/g$ = 2000 seconds.

For comparison we can estimate the performance if the flow is completely frozen at stagnation conditions. At 2 eV and 10^3 atm the polyethylene is ~30% ionized. If the exhaust flow is frozen, the dissociation and ionization energy per particle increases from 3.3 eV to 6.7 eV per particle, and the efficiency drops to η_T = .47. The frozen flow specific impulse is then 1600 seconds. One way to view this result is to state that a PET thruster with an equilibrium flow nozzle can achieve a given specific impulse at a lower stagnation temperature and higher efficiency than a frozen flow device.

Experimental Apparatus

The relatively high impulse bit of the PET thruster in these experiments, typically 0.1 N-sec, greatly simplifies the task of measuring thrust. The thruster, with mass M = 2.5 kg, is attached to a simple linear thrust stand (Figs. 3 and 4), and the recoil velocity V of several cm/sec is measured after each shot. The impulse bit is then simply $\int T dt$ = MV[N-sec]. The thruster is mounted on a linear bearing and hardened steel shaft, and current is fed through flexible strips of copper mesh. A shorting bar in the capillary is used to verify zero thrust contributions from magnetic fields. The recoil velocity is measured by a linear inductive RF transducer

[Bently Nevada Model 21504, 8 V/mm] and steel target, so that micron-level motions can be detected. The accuracy of this system is better than 5%. The transducer output signal is recorded on a digital oscilloscope at 2 μsec/point and is graphically differentiated to give the initial recoil velocity V (Fig. 5). Alternatively, the recoil velocity can be determined by fitting the output signal to a waveform $x(t) = x_o e^{-\alpha t} \sin\omega t$, where α, x_o and ω can be easily measured (Fig. 5). Both techniques give equivalent results.

The thruster is sealed to the vacuum tank by a thin (0.4 mm) flexible diaphragm of rubber fabric, located at the nozzle throat (Fig. 4). This arrangement keeps the electrical connections outside the vacuum tank, greatly simplifying the design of the high voltage insulation. The load on the thruster and diaphragm caused by atmospheric pressure is counterbalanced by coil springs. The natural period of the thruster mass-spring system is 0.090 sec, and the damping of the system is low (Fig. 5).

Since the thrust measurement is a vital performance parameter a means of calibrating the thrust stand has been devised (Fig. 6). A physical pendulum of mass m is constructed to rotate about point O, and impact the thruster mass m at a radius r. The impact point at r is designed to be the center of percussion about O so that no impact forces are transferred to the suspension structure. The pendulum and thrust stand are then considered a purely rotational system, with angular momentum about O being conserved.

The pendulum velocity immediately before and after impact is found by passing the focussed beam of a helium-neon laser through a grid of equi-spaced slits (50 line/inch Ronchi Ruling), and measuring the chopping frequency of the transmitted beam (Fig. 6). All other fixed characteristics of the pendulum such as the moment of inertia are known, so that the net momentum transferred to the thrust stand can be calculated. Simultaneously, the recoil momentum of the thrust stand is found using the position transducer (Fig. 5). Comparison of the two measurements yields a calibration constant that is applied to all subsequent thrust data obtained using the transducer method. This constant is 0.985, indicating that the thrust stand measurement system is inherently accurate to within 1.5%.

The energy storage pulse forming network of these experiments is composed of L-C sections, each section consisting of a 1.1 μH inductor and two 29 μF high voltage capacitors (Aerovox PX80D18), with a characteristic impedance of .140 ohms. Experiments are performed with 1, 3 and 6 sections, giving current pulse lengths of 15, 48 and 100 μsec (Fig. 2). In all cases the load impedance is well matched to the source, resulting in efficient energy transfer to the discharge.

PET thruster performance is based on the energy delivered to the discharge in the first half cycle, typically 92% of the stored energy, and is determined by integration of the currrent and voltage at the thruster terminals. Thruster current I is measured with a Rogowski loop, passively integrated with an RC = 2.8 msec integrator. Terminal voltage V is measured with a 935:1 resistive divider. Both I and V are recorded at 2 μsec/point, enabling the product IV to be internally computed, integrated, and displayed on the scopeface (Fig. 7).

The propellant is commercial high density black polyethylene. The ablated mass Δm is determined by weighing on a sensitive scale (Voland Model 220R) to an accuracy of 0.5 mg, and weighing again after firing 10-20 shots at fixed conditions. The cathode and nozzle are weighed similarly. The nozzle ablation is quite small, and visual inspection after 100 shots on the nozzle has shown no visible erosion. The cathode loss is less than 15% of the total, and is estimated not to participate in the discharge. The capillary loss is typically accurate to 5%, whereas the cathode and nozzle erosion data are less precise due to the smaller mass losses.

The thruster exhausts into a vacuum tank of 12 cm ID by 125 cm long, with access ports located every 25 cm downstream (Figs. 8 and 9). In addition, an access port is located on the centerline at the far end with provision for a 200 cm long adjustable probe mount. Several probes can be inserted into the tank on one shot for exhaust measurements, and up to three probes can be located at one axial downstream position.

Three time-of-flight techniques have been employed to measure exhaust velocity: ion saturation probes; piezo-electric stagnation pressure probes; and photodiode sensors (Fig. 9). The velocity measured by each of these techniques is generally in agreement. A description of each technique is presented below.

The ion saturation probe is a double Langmuir configuration consisting of two identical wires, 0.23 mm diameter, embedded in epoxy. The wires protrude from the surface approximately 0.8 mm, and are spaced 1.5 mm apart. Exhaust plasma stagnates on the probe surface, providing a conductive path across the wires, which are biased with a 29 V battery.

In this configuration, the Langmuir probe signals show large, erratic fluctuations in amplitude. Such behavior is attributed to local cooling of the plasma due to evaporation of the epoxy material in the vicinity of the wires. However, the mean amplitude of the signal is consistent with a stagnation plasma at 2.4 eV with a density of $\sim 10^{17}$ cm^{-3}. Arrival times as determined by the onset of the satur ion current signal, are in complete agreement with those obtained using the pressure and photodiode probes.

The stagnation pressure probe (Fig. 9) consists of a sensitive piezoelectric transducer (PCB 102A12, 44 psi/volt), mounted on the vacuum tank centerline on a moveable support. The transducer tip is covered by mylar tape for protection from the discharge plasma. Typical probe signals are shown in Fig. 10 for two probe positions, showing that a time-of-arrival can be clearly measured for each shot. These times are plotted and the mean slope is measured graphically to determine the exhaust velocity.

A third time-of-arrival technique employs simple red-sensitive diodes to record the plasma flash on the tip of a transparent plastic stinger (Fig. 9). Th probe is located downstream from the nozzle exit plane and records a spike of radiation when fast moving plasma strikes the probe (Fig. 11). Again, the arrival times for different axial probe positions are plotted to determine the exhaust velocity.

The total mass of the ambient gas in the tank at $P_{amb} \sim .003$ torr is a small fraction of the exhaust mass Δm, so that the pressure transducer and the photodiode probes respond to the exhaust mass without interference of the background gas. The data from all three probes predict velocities consistent with each other to within 10%.

Experimental Results

Several series of 10 shot tests were run using polyethylene propellant. The delivered energy ranged from 1.78 to 1.89 kJ for 15 and 48 μsec pulses, and was 3.98 kJ for 100 μsec pulses. The capillary diameter was 4.3 mm in all cases.

The capillary length and pulse length were varied to permit the thruster to run in an unsteady or quasi-steady mode, depending on the number of acoustic travel times during the current pulse, given by $ct_p/2\ell$. The values of this parameter are given in Table I below.

Table I. Experimental Pulse Lengths for Polyethylene

Test Series	Pulse Energy, kJ	Pulse length, μsec	Capillary length, cm	$ct_p/2\ell$
1.	1.80	15	15	0.4 Unsteady
2.	1.78	48	5.5	3.5 Quasi-steady
3.	1.89	48	4.5	4.3 Quasi-steady
4.	3.98	100	4.5	8.9 Quasi-steady

A summary of the performance results is shown below in Table II. The estimated precision of the Table II measurements is:

1. Recoil motion x(t). Impulse bit is measured to 5%.
2. Exhaust probe time-of-flight, accurate to 10%
3. Current, accurate to 3%.
4. Voltage, accurate to 3%.
5. Mass loss Δm, accurate to 6%.

Discussion of Results

The probe measurements of exhaust velocity give results which are consistent with our understanding of the physics of the discharge. In the unsteady mode case (Series 1), the current impulsively heats the discharge plasma which is then accelerated as the temperature decays. The measured exhaust velocities are 20-21 km/sec. The quasi-steady cases (Series 2-4) achieve nearly steady state conditions, and hence a higher mean sound speed for the duration of the pulse. The exhaust velocities are correspondingly higher: 26- 28 km/sec.

What evidence do we have that the exhaust velocities measured correspond to electrothermally heated and accelerated propellant mass, and not to some relatively

Table II. PET Thruster Performance with Polyethylene, 10 shot averages.

Delivered energy, E_D	1.80	kJ	1.78	kJ	1.89	kJ	3.98	kJ
Maximum current, I_M	23	kA	17	kA	15	kA	15	kA
Pulse width, half max	15	μsec	48	μsec	48	μsec	100	μsec
Impulse bit, $\int Tdt$	.20	N-sec	.095	N-sec	.086	N-sec	.189	N-sec
Exhaust velocity:								
Pressure transducer	21	km/sec	28	km/sec	-	-	-	-
Photodiode probes	20	km/sec	26	km/sec	26	km/sec	27	km/sec
Capillary ablated mass	20	mg/shot	6.5	mg/shot	5.3	mg/shot	10.8	mg/shot
Electrode + nozzle ablated mass	NA		NA		~0.9	mg/shot	~2.0	mg/shot

low-mass precursor or shock wave? First is the time response of the pressure and photodiode probes (Figs. 10 and 11), which display a pulse width about equal to that of the current pulse. This suggests that the probe is responding to the momentum flux generated in the nozzle. Second is the nearly comparable velocity measured by the pressure and photodiode probes. Third, we have theoretical predictions of both the exhaust velocity and probe stagnation pressure, described below, which give reasonably good agreement with the measured values.

Computational Model

The predicted performance of a PET thruster capillary with polyethylene has been modeled numerically [1]. Inputs to the GT-Devices code include polyethylene chemistry [4], plasma resistivity, capillary geometry, and the experimentally measured current and voltage waveforms. Because the plasma resistance is known, this can be used to calibrate the resistivity model used in the code, with the result that the plasma resistivity is close to that given by the Spitzer model [5].

The most sensitive quantity calculated by the model is the ablated mass, which varies as T^4 (blackbody) radiation in the capillary. A calculation of the ablated mass time history is given by the computational model for a 2 kJ shot with polyethylene in the quasi-steady mode (Fig. 12). The model predicts a total ablated mass of 6.2 mg, in close agreement with the average measured value of 6.5 mg per pulse. At the end of the current pulse, the model predicts that only 4.1 mg has been ejected. A significant fraction is apparently thus exhausted at a much reduced velocity, characteristic of the lower sound speed in the afterglow.

Predicted performance curves for a polyethylene 2 kJ shot in the quasi-steady mode are shown in Fig. 13 for the capillary pressure, temperature, and sound speed. The stagnation sound speed c_o in the capillary is ~9 km/sec during the current pulse, during which time $\gamma = 1.2$. Assuming adiabatic flow, with constant $\gamma = 1.2$ in the nozzle, the exit Mach number is then $M \sim 4.7$, corresponding to the nozzle area ratio of 95. At this Mach number the temperature drops by a factor [6]

$$\frac{T_{ev}}{T} = 1 + \frac{\gamma-1}{2} M^2 = 3.2$$

The sound speed thus drops by a factor of about $\sqrt{3.2} = 1.8$, to $c = 4.8$ km/s. The corresponding predicted exhaust velocity is $u_e = Mc = 22$ km/sec, approximately the measured exhaust velocity.

More evidence for high Mach number flow lies in the pressure probe response (Fig. 10), which shows a maximum signal of about 2 atmospheres. The thruster stagnation pressure can be estimated from the measured impulse bit, throat area, and pulse length [6]:

$$p_o \sim \frac{\int T dt}{C_F A^* t_p} \sim 710 \text{ atm}$$

for $C_F \sim 2$ and $t_p \sim 50$ μsec. This pressure is in good agreement with that predicted by the computational model (Fig. 13). If we assume that a normal shock sits on the pressure probe tip, then the probe response P_{oy} to the shocked gas is given by [7]:

$$\frac{p_o}{p_{oy}} = \frac{\left(1 + \frac{\gamma-1}{2} M^2\right)^{\frac{\gamma}{\gamma-1}}}{M^2}$$

The probe peak amplitude of 2 atm corresponds to $P_o/P_{oy} = 350$. For $\gamma = 1.2$, this pressure ratio indicates $M \sim 6.3$, corresponding to a flow velocity of 25 km/sec for $c_o = 9$ km/sec. This value is consistent with the exhaust probe time-of-flight measurements.

Based on the numerical model, the measured exhaust velocities are consistent with a highly supersonic, adiabatic nozzle. Consistent with this model, the pulse width detected by the pressure transducer remains roughly constant with distance from the nozzle. This non-dispersive feature is characteristic of a high velocity puff of gas with a low sound speed. Furthermore, the measured velocity is consistent with adiabatic expansion of a polyethylene plasma with a stagnation temperature of 2.5 eV and a stagnation pressure of ~700 atmospheres. The stagnation enthalpy is 340 kJ/gram for polyethylene plasma [4], which would then fully expand to 26 km/sec, a value close to that measured by the velocity probes.

Performance Measurements

The thrust to power ratio [N/kW] can be evaluated in the form

$$\frac{T}{P} \text{ [N/kW]} = \frac{\int T dt}{\int P dt/1000} = \frac{\int T dt}{E_D \text{[kJ]}}$$

The values of T/P for the 2 kJ shots (Table II) are shown below in Table III. The velocities shown are those measured by the velocity probes for the mass exhausted during the current pulse.

The thruster efficiency η_T is conventionally defined as

$$\eta_T = \frac{\text{exhaust kinetic energy}}{\text{energy delivered}} = \frac{1/2\ m u_e^2}{E_D}$$

For a pulsed device, the exhaust kinetic energy is

$$1/2\ m u_e^2 = \int 1/2\ \dot{m} u_e^2 dt$$

Table III. Measured Thrust to Power Ratio for Polyethylene at 2 kJ

		u_e(Probe)	T/P
1.	Unsteady, 15 μsec pulse	21 km/sec	.10 N/kW
2.	Quasi-steady 48 μsec pulse	27 km/sec	.053 N/kW
3.	Quasi-steady 48 μsec pulse	26 km/sec	.046 N/kW
4.	Quasi-steady 100 μsec pulse	27 km/sec	.048 N/kW

where the integral is continued past the end of the current pulse to account for the discharge afterglow, during which propellant evaporation decays to zero. Unfortunately the time dependence of $\dot{m}$ and u_e are not known, so that we must define the efficiency in terms of impulse bit as:

$$\eta_T = \frac{[\int T dt]^2}{2\Delta m E_D}$$

where Δm is the capillary ablated mass, and is used to define the specific impulse by

$$I_{sp} = \frac{\int T dt}{g \Delta m}$$

The data from Table III above can therefore be used to evaluate η_T and I_{sp} for Series 1-4, shown below in Table IV.

Table IV. PET Thruster Efficiency and I_{sp} for Polyethylene at 2 kJ

		η_T	I_{sp}
1.	Unsteady 15 μsec pulse	.56	1000 sec
2.	Quasi-steady 48 μsec pulse	.39	1500 sec
3.	Quasi-steady 48 μsec pulse	.37	1600 sec
4.	Quasi-steady 100 μsec pulse	.42	1750 sec

The specific impulse values in Table IV are about half of those indicated by the exhaust probe velocity measurements. This is primarily because the mass fraction ejected in the afterglow tail of the pulse has significantly lower velocity than the fraction ejected during the pulse. This is expected since the afterglow plasma is cooler.

Conclusions

A PET thruster has been built and tested on a thrust stand, giving repeatable results over a series of shots. Exhaust velocities for polyethylene propellant vary from 20 to 27 km/sec, as measured by exhaust probes. These velocities are consistent with computational predictions of capillary conditions with an adiabatic expansion to high Mach number in a conical nozzle. Single pulse specific impulse and efficiency measurements based on ablated mass show a thruster efficiency of 37-56% in the 1000-1750 second range. We believe that an understanding of loss mechanisms in the discharge would lead to an improved design with a thruster efficiency of 70-80%.

Acknowledgements

We gratefully acknowledge the interest and support of F. Terdan and S. Wang of NASA-Lewis Research Center, and of D. Byers and W. Hudson at NASA Headquarters. This work was supported in part under NASA Contracts NAS3-23779 and NAS3-23866.

References

1. Burton, R. L., Goldstein, S. A., Tidman, D. A., and Winsor, N. K., "Theory of the Pulsed Electrothermal Thruster", AIAA Paper No. 82-1952, AIAA/JSASS/DGLR 16th International Electric Propulsion Conf., New Orleans, November 17-19, 1982.
2. Zel'dovich Y. B., and Raizer, Y. P., Physics of Shock Waves and High-Temperature Hydrodynamic Phenomena, Vol. I, Academic Press, New York, 1966, p. 406 ff.
3. Herzfeld, K. F., et al., Fundamental Physics of Gases, Number 7, Princeton Aeronautical Paperbacks, C. duP.Donaldson, ed., Princeton University Press, Princeton, NJ, 1961.
4. SESAME Equation of State Library, Report LASL-79-62, Los Alamos Scientific Laboratory, Los Alamos, NM.
5. Spitzer, L., Physics of Fully Ionized Gases, 2nd ed., Interscience Publishers, New York, 1962.
6. Shapiro, A. H., The Dynamics and Thermodynamics of Compressible Fluid Flow, Vol. I, The Ronald Press Company, New York, 1953.
7. Burton, R. L., Goldstein, S. A., Hilko, B. K., Tidman D. A., and Winsor, N. K., "Investigation of a Pulsed Electrothermal Thruster", Final Report No. NASA CR-168266, NASA Lewis Research Center, October 1, 1983.

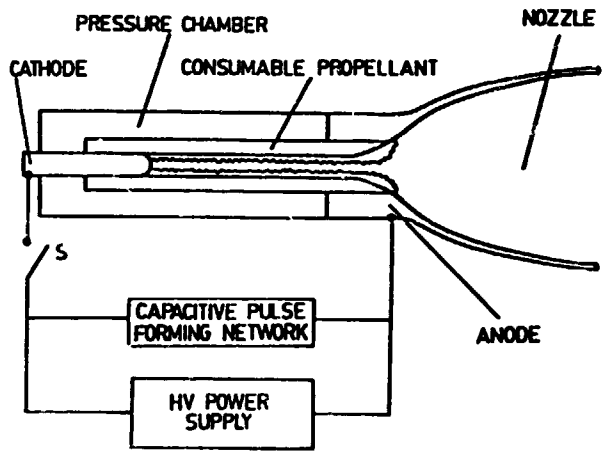

Fig. 1. PET Thruster System Schematic

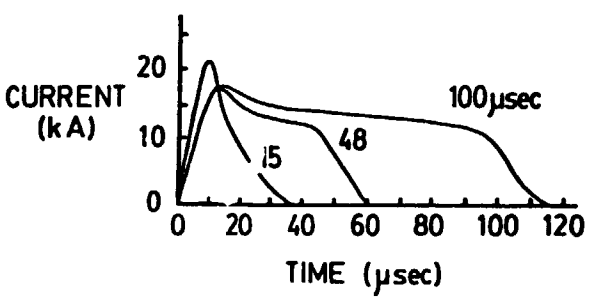

Fig. 2. PET Thruster Current Waveforms

Fig. 3 PET Thrust Stand

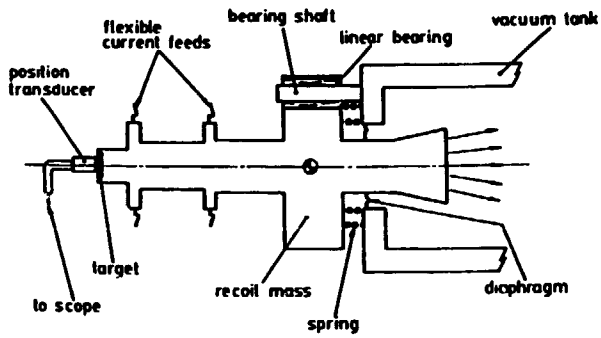

Fig. 4. PET Thrust Stand Schematic

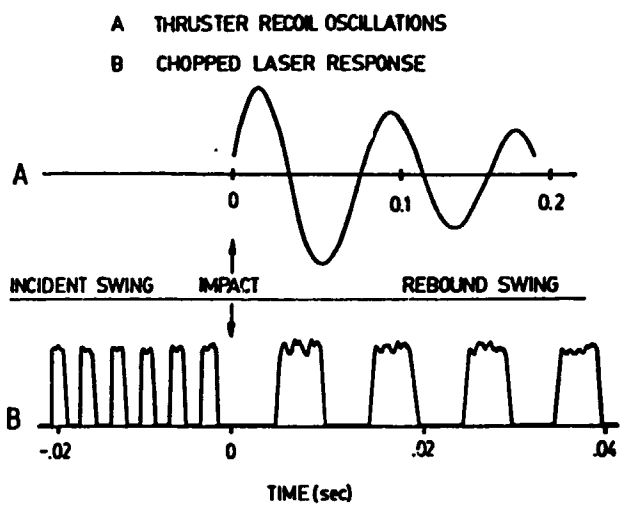

Fig. 5. Thrust Stand Recoil and Calibration Response

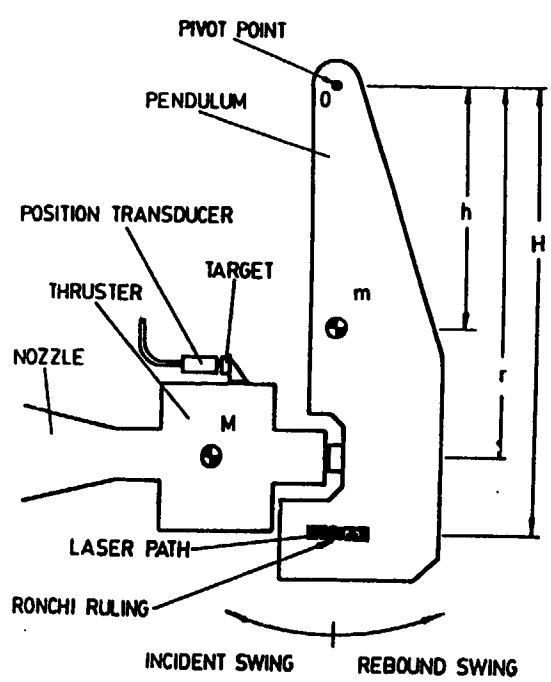

Fig. 6a. Thrust Stand Calibrator Schematic

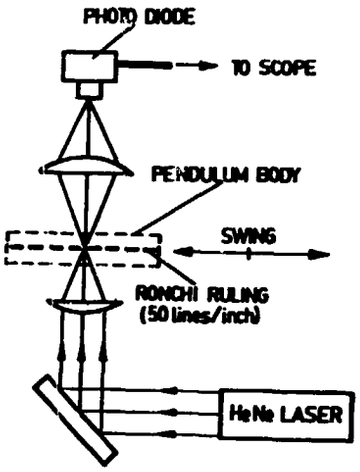

Fig. 6b. Calibrator Optical Schematic

Fig. 8. Vacuum Tank with Access Ports

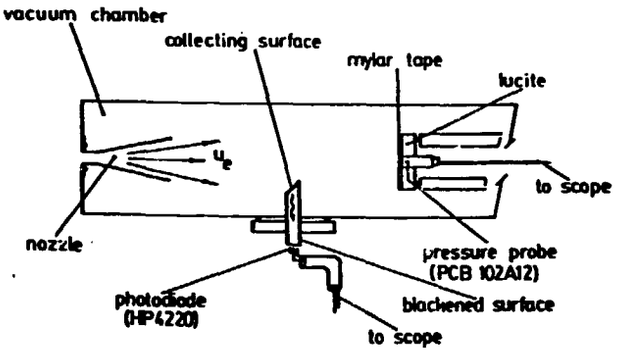

Fig. 9. Exhaust Flow Diagnostics

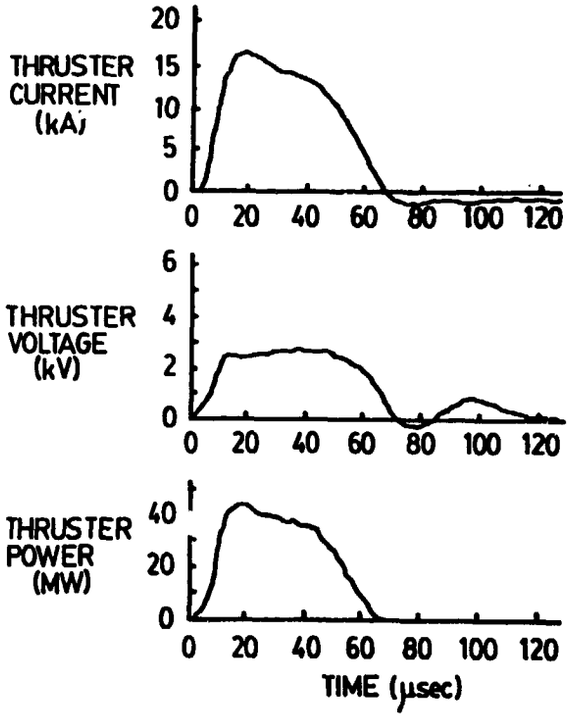

Fig. 10. Exhaust Pressure Probe Response at Two Positions

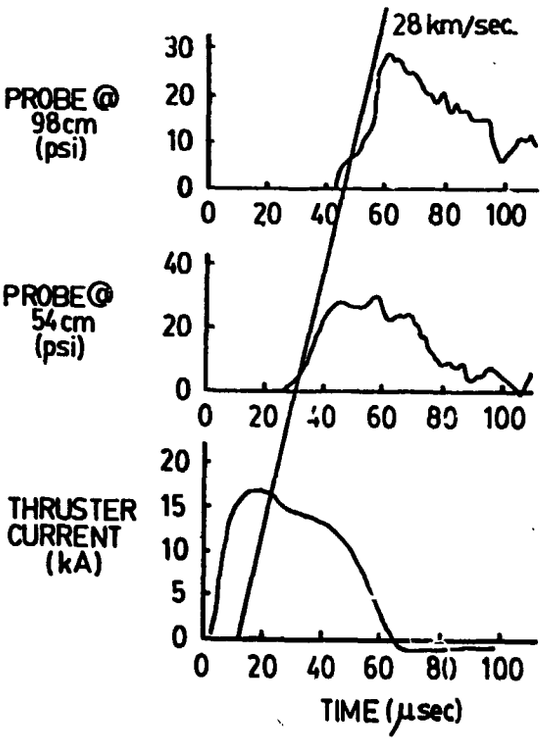

Fig. 7. PET Power Input Waveforms

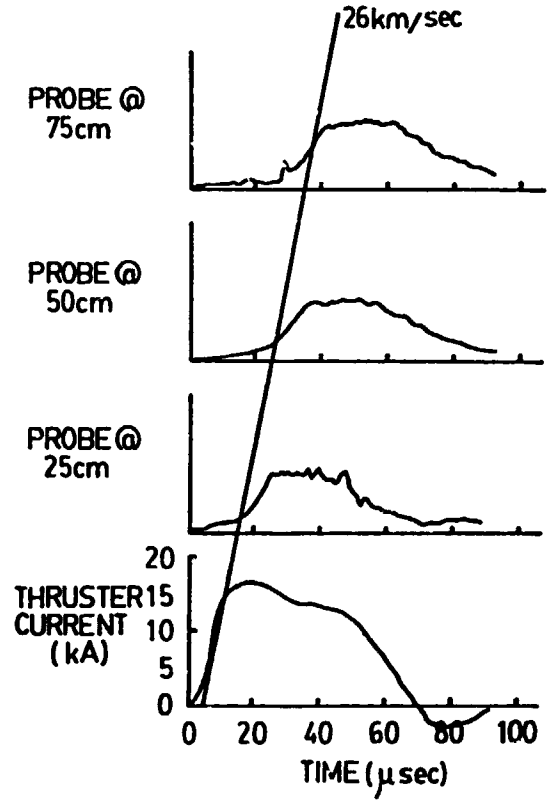

Fig. 11. Exhaust Photodiode Probe Response at Three Positions

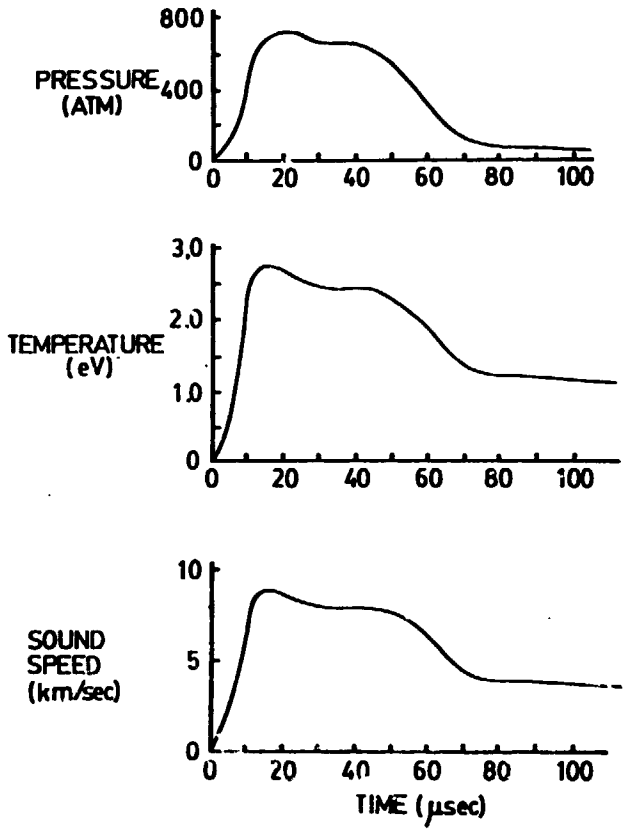

Fig. 13. Calculated Capillary Performance, 2 kJ shot

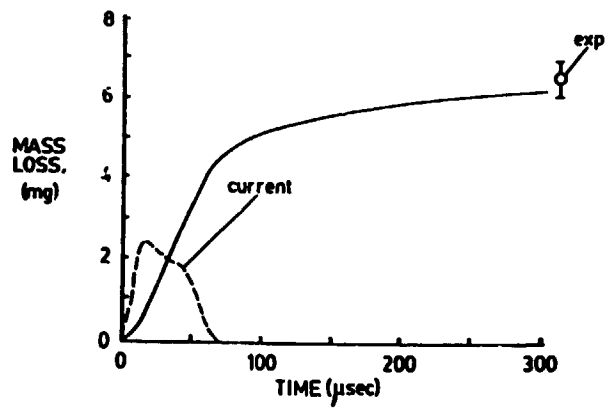

Fig. 12. Calculated and Experimental Polyethylene Mass Ablations